Chapter

Design, Simulation and Analysis of the Propulsion and Control System for an Electric Vehicle

Muhammet Tahir Guneser, Mohammed Ayad Alkhafaji and Cihat Seker

Abstract

The problems of global warming, a decrease of the available natural resources and many other problems in the world that happen recently become the major cause for increasing the demand for a new type of vehicle. That vehicle can be an environmental friend and so that a new generation of vehicles has been invented and tried to solve and avoid many problems. In this chapter, the proposed system is called the Multi-Converter/Multi-Machine system (MCMMS) which consists of two Synchronous Reluctance Motor (SynRM) that drive the two rear wheels of Pure Electric Vehicle (PEV). The SynRM speed and torque are controlled by using three different strategies of the PID controller. The PSO algorithm has been used as an optimization technique to find the optimal PID parameter to enhance the drive system performance of the PEV. In this system, the space vector pulse width modulation inverter for voltage source (VS-SVPWMI) has been employed to convert the DC battery voltage to three-phase AC voltage that feeds the SynRM motor in the PEV. The linear speed of the vehicle is controlled by an Electronic Differential Controller (EDC) which gives the reference speed for each driving wheel which depends on the driver reference speed and the steering angle. The specified driving route topology with three different road cases has been applied to acting and show the resistive forces that affected on the PEV during its moving on the road. In addition, to test the efficiency and stability of the PEV on the roads. Hence, this chapter has a full design, simulation and several comparison results for the propulsion electric vehicle system and it has tested implemented in the Matlab/Simulink environment version R2020a.

Keywords: SynRM, SVPWM, Inverters, d-q Transformation, Electric vehicle, EDC, PSO algorithm, Driving cycle, Matlab/Simulink

1. Introduction

Environmental pollution and global warming resulting from the combustion of petroleum products in mechanical vehicles have pushed many companies to use electric vehicles (EV) that rely on clean alternative energy instead of petroleum energy. Besides, customers' interest in the increasing demand for EV due to their efficiency and modernity [1–4]. This prompted several companies to develop their

products and expand their research studies on them so that they become as competitive as possible in mechanical vehicles. EVs are not only more efficient than their counterparts that operate on internal combustion engines, but they are also the best option to reduce pollution resulting from greenhouse gas emissions and noise, as they produce emissions at a rate less than half of what conventional cars produce.

EVs are environmentally friendly, as they do not emit carbon emissions of any kind and do not emit smoke or exhaust, and therefore, they protect the environment, especially in crowded cities [1–9]. It also works with recycled and reused batteries, to store energy in EVs, and finally it is suitable for cities where EVs are characterized by their quietness as they do not have an annoying engine sound, and suitable for crowded cities, due to the ease of controlling them from start and stop. Moreover, EV is not currently a detection; It was first proposed in the mid-nineteenth century. Although they have been around for a long time, they have not become as popular as Internal Combustion Engine (ICE) cars in the narrative of recent years [2, 4, 9–13], due to the main obstacles to electric vehicles as they are expensive, especially high-voltage batteries that are expensive, limited in range, and have little infrastructure. Charging stations as well [2]. The technological development of countries over the years, infrastructure and the EV of industries that led to the arising of environmental contaminate here then the need began to arise for the presence of vehicles that are concerned in that concern. The environmental side and from here began and the urgent need for EV to increase.

The market demand for EVs is expected to increase very shortly is anticipated to increase. Nowadays in many European and Eastern Asia countries and North America has a major interest in the development and the use of EVs [1–3]. They use EVs as taxis and as personal cars to move around within the city for the presence of trains and planes to move for the long distant places and a major concern now to make EVs move in the out-city range. Many EVs are used in cars as taxis Because EVs are a low cost compared to mechanical vehicles and charging stations are solar cells that transform solar energy into electrical energy [1, 2, 4–6]. It is one of the following sources of clean energy.

The manufacture and construction of electric vehicles vary from company to company, determined according to the needs and specifications required for the industry. There are many types that can be explained as follows: The first type is considered one of the oldest types which are still adopted in the industry and it contains one electric motor that is connected to the rear wheels and this type is called conventional electric vehicles or “classical EV system”. The second type of system will be studied and analyzed in this chapter, which is based on two electric motors in the rear wheels of the EV, in which each engine operates separately from the other and is controlled by smart systems and this type is called “ propulsion EV system “.The third type is the same design as the second type of electric vehicle, but the propulsion mechanism “electric motors” is attached to the front wheels of the vehicle and this type is called “ traction EV system “.The fourth type of electric vehicle is a four-wheel drive using two electric motors. The first is on the axle of the rear wheels and the second is on the axle of the front wheels and each of them works separately with a specific control mechanism. This type is called a “ four-wheel two motors EV system “. The last type of electric vehicle, which is four-wheel drive, using four electric motors, is distributed over the four tires of the vehicle and works separately, and this type is called “four-wheel EV system” [10]. In general, there are two types of electric vehicles which are Hydride Electric Vehicles (HEV) and Pure Electric Vehicle (PEV). These two types are considered as the major types of EV and minor types are divided from these two types depending on different aspects related to the driving system, configuration, costumers order, and other concerns depend on the designing specification.

DOI: http://dx.doi.org/10.5772/intechopen.98873

The most current invention in the type of vehicle manufacturing EV [1–4]. The PEV are completely different from traditional "mechanical vehicles", although they operate on electrical energy starting from fuel and mechanical fuel engines, the internal structure of them depends on electronic circuits, transducers, and batteries. As well as the entry of artificial intelligence into the manufacturing process to control and control the electronic devices they contain [4, 13, 14]. Besides, in this type instead of using the gearbox, the Electronic Differential Controller (EDC) is designed and used to control the EV on the road. EVs that categorized according to the job of the drive system the many known electric drive systems that have been utilized in EV is induction motors (IM), brushless, DC motors (BLDC), permanent magnet synchronous motors (PMSM), switch reluctance motor (SRM) and other DC motors [15–20].

One of the most important things that must be considered when designing and simulating EVs is the method of controlling the electric vehicle on the road under different conditions to ensure the efficiency of the electric vehicle. As well as artificial intelligence and the application of new mathematical algorithms that help advance the manufacture of electric vehicles. The speed control of the electric motor in terms of rotation speed and torque is one of the most important factors that help in the success of electric vehicle design [2–4, 17–23]. As well as studying the forces affecting the vehicle on the street and applying artificial intelligence algorithms to get rid of them to make the electric vehicle compatible with all road conditions and the influence of external factors on it [13, 14].

The proposed EV system in this chapter called propulsion type EV which are consists of two motors that ensure the drive of the two rear driving wheels. Each motor is drive separately from the other by SynRM and the whole system is controlled by an electronic differential that guarantees the robustness of the vehicle. This vehicle system MCMMS. This type of EV is the most recommended type by the mechanical experts because of slipping issues in the curvature and high road in this type of vehicle **Figure 1** shows an EV with a rear-wheel drive system [4, 23]. Multiple intelligence theories and algorithms have been applied to control the vehicle's electric motor. Likewise, the design and analysis of EDC will be used to control the vehicle's speed during a bad road on road. In addition, a complete

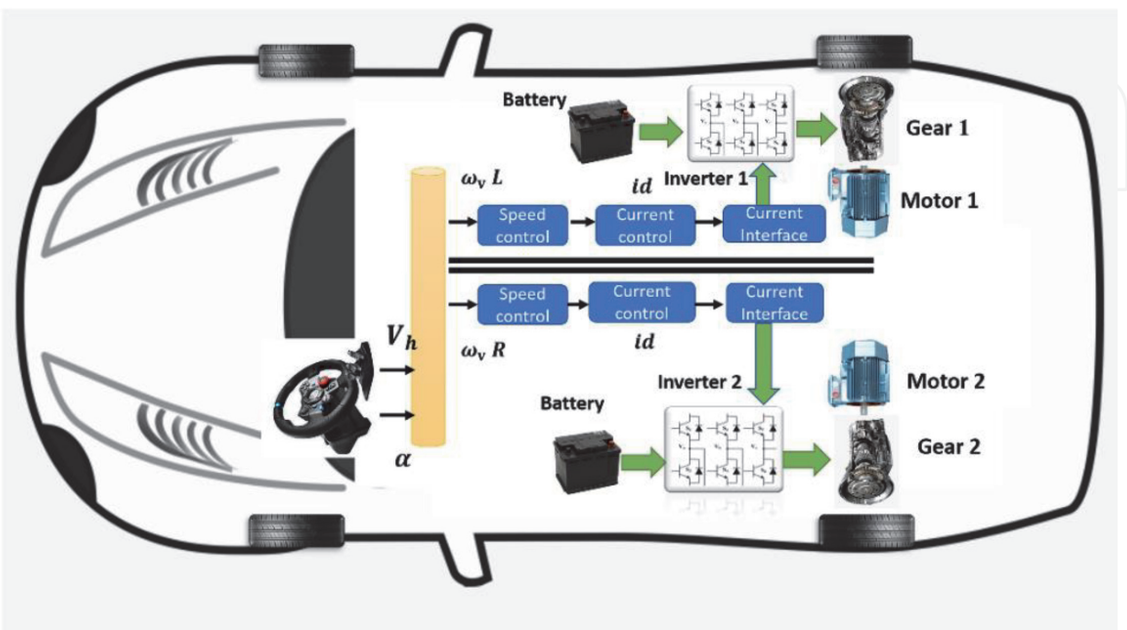

Figure 1.
The propulsion EV platform system.

simulation of the road with three different roofs to ensure the efficiency of the electric vehicle. The above will be explained in detail during this research with the scientific results and comparisons for each part designed in this EV [4–7, 24–31].

2. The mathematical modeling of the system

2.1 SynRM mathematical model

SynRM is one of several synchronous machines and it is one in every of numerous synchronous machines, the SynRM rotor structure has synthetic without winding or magnet fabric. As an evaluation among SynRM with other sorts of reluctance Electric Vehicles (EVs) like: IM, BLDC motor and switch reluctance motor SRM. The quit result suggests that SynRM is precise in production, easy form. In addition, it has an extraordinary residence like low torque average, larger torque pulsation and occasional energy factor [6, 7].

Undoubtedly, the SynRM may additionally moreover deliver an excessive solid performance in assessment with other AC drives compared with IM. As noted earlier, the SynRM is a type of synchronous machine that does not have any winding or permanent magnet at the rotor and salient poles, it has a fragmented rotor of several barriers. The cause for made the reluctance motor rotor form laminated axially metallic it has to dominate low torque response and incorrect electricity thing, notwithstanding the truth that older variations of reluctance motor have lacked this period of producing [5–7]. The stator-winding format of SynRM is quite much like the IM. Whereas the rotor shape of SynRM is quite precise from IM, it is not caged rotor or twisting and does not have any magnetic fabric, it has only laminated obstacles which designed in a complex manner, and an optimized to have a pinnacle quadrature axis compliments and non-direct axis jealousy, once the magnetic concern goes with the flow in the stator winding and in step with the rotor structure it's far a low and high hesitation vicinity and they represent almost the magnetic poles [5–16].

The rotor layout in SynRM is rotated to reach the low reluctance regions and drifting away of the immoderate reluctance areas inside the equational time of rotation, the purpose of this work method to acquire the magnetic location synchronous speed. The stator machine to each of SynRM and IM is the same signal in the rotating frame. The SynRM does no longer want any magnetic or winding substance at the rotor form which makes the motor rugged, introduction simplicity, the most inexpensive rate of manufacturing, better torque according to unit quantity possibility, working at most high speeds functionality which makes the SynRM, and the rotor windings Failing to end result from easy control strategies, and the decline's minimization create SynRM an appealing and famous desire for several business and care programs due to all of these awesome and splendid traits [7, 12].

The earliest variations of SynRMs are used immediately a caged rotor, the most crucial cause that pristine SynRMs do no longer have starting torque attributes, however now the modern-day SynRM and using the most updated styles of inverters, area orientation manage FOC generation at the side of using Pulse Width Modulation (PWM) method deliver a convenient approach for manage, so without any rotor cage that the tool may also be initiated. The velocity variable parameters have utilized in SynRM motor system layout to correct the motor speed strength because of numerous factors like electricity conservation, manage the situation, velocity, and enhancement of the brief response traits [6, 7–12, 28, 31].

The aim of a motor tempo controller is to take a sign representing the reference tempo and to strain the motor at that reference velocity. Although, the control

machine consists of velocity that been comments from the machine, a SynRM, a voltage supply location vector inverter, a controller, and a speed placing the device [6, 7, 22]. The fundamental reason for the use of comments in one's systems is with a purpose to gain a reference-thing irrespective of any variation or exclusive problem within the traits the tool decrease returned to the reference issue. **Figure 2** is displayed the SynRM rotor flux barrier and IM motor rotor cage. In addition, the SynRM motor can be located from its d-q stationary axis the same circuits as in **Figure 3**.

The SynRM version is pretty like the induction motor IM. The difference is by way of neglecting the rotor losses from the IM equations. The SynRM's version is described via (Eqs. (1)–(4)) [5–7, 16].

$$V_d = R_s I_d + \frac{d\lambda_d}{dt} - \omega_r \lambda_q \tag{1}$$

$$V_q = R_s I_q + \frac{d\lambda_q}{dt} + \omega_r \lambda_d \tag{2}$$

$$\lambda_d = L_d I_d \tag{3}$$

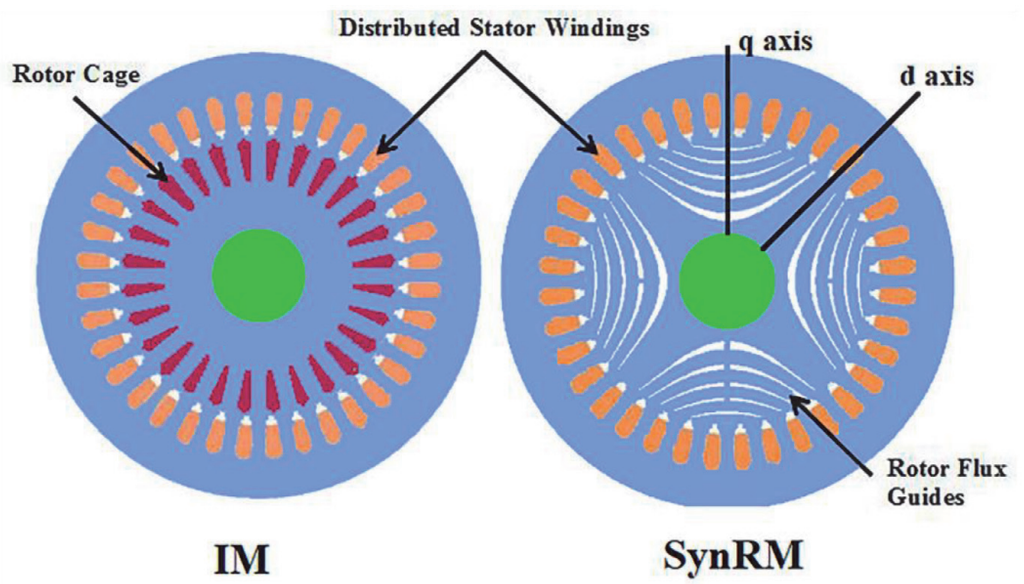

Figure 2.
The machinal contents of SynRM and IM.

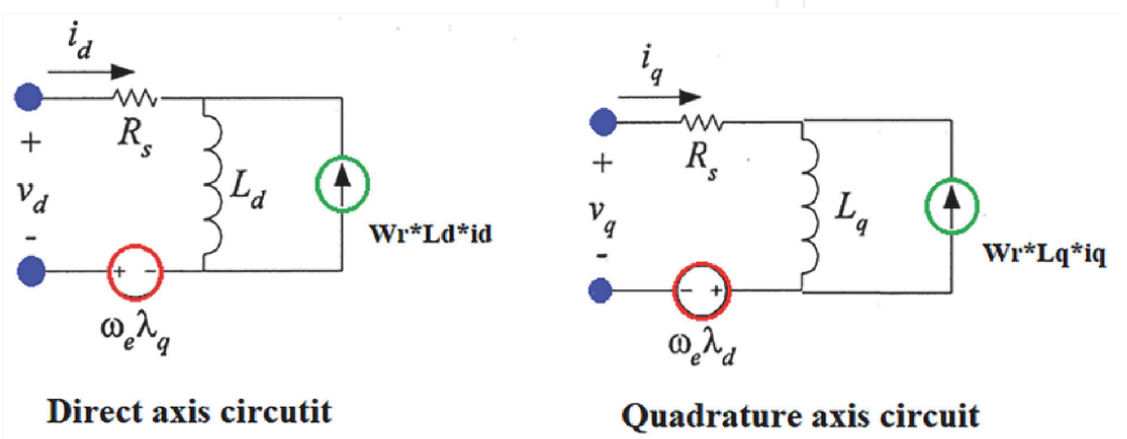

Figure 3.
The equivalent circuit of d axis and q axis for SynRM.

$$\lambda_q = L_q I_q \tag{4}$$

By both of each (Eqs. (3) and (4)) the over shift speed could be acquired as will detect in (Eqs. (5) and (6)) as following:

$$\frac{d\lambda_d}{dt} = V_d - R_s I_d + \omega_r \lambda_q \tag{5}$$

$$\frac{d\lambda_q}{dt} = V_q - R_s I_q - \omega_r \lambda_d \tag{6}$$

From (Eq. (5)) the change-speed rate of the direct axis current could be gained in (Eq. (7)).

$$\frac{dI_d}{dt} = \frac{1}{L_d}\left(V_d - R_s I_d + \omega_r L_q I_q\right) \tag{7}$$

And with (Eq. (6)) the change-speed rate of the quadratic axis current could be gained in (Eq. (8)).

$$\frac{dI_q}{dt} = \frac{1}{L_q}\left(V_q - R_s I_q + \omega_r L_d I_d\right) \tag{8}$$

Besides, to obtain the torque of SynRM we have used in (Eq. (9)).

$$T_e = \frac{3}{4}\frac{P}{2}\left(L_d - L_q\right) I_d I_q \tag{9}$$

The of speed rate can be acquired by (Eq. (10)).

$$\frac{d\omega_r}{dt} = \frac{P}{J}\left(T_e - T_L\right) \tag{10}$$

The Laplace transformation of the torque is given as follows by (Eq. (11)).

$$T = \frac{3}{2}\,P\left(L_d - L_q\right) i_d i_q - \left(B\omega_r + J\frac{d\omega r}{dt}\right) \tag{11}$$

Table 1 show the SynRM parameters that used in the design. These parameters are the same parameters for the IEv4 motor for the ABB company.

Parameter	Parameter value	Units
Ld	6.0645	mH
Lq	0.910	mH
Rs	0.0265	Ohm
J	0.245	Kgm^2
B	0.0000009	N.m.s
P	2	poles

Table 1.
The main parameters of the SynRM.

2.2 Voltage source inverter

Inverters are power electronics systems that turn the DC voltage from a battery or some other DC source into alternating current voltage, which may be single-phase, two-phase, or three-phase, depending on the inverter configure ratio. Inverters that feed synchronous motors are mainly used in variable voltage and variable frequency applications for high-performance variable speed [4, 6, 7]. SVPWM is the most widely used PWM technique due to its high output voltage, low harmonic distortion, and superior efficiency as compared to other types of inverters. The SVPWM inverter is a complex scheme that produces a high voltage fed to the generator, resulting in a low overall harmonic distortion [4, 6, 15, 16]. The aim of the various modulation schemes is to provide a variable output with a maximum fundamental factor that can generate as few harmonics as possible. The switching instants are calculated using the SVM scheme, which is based on the representation of the switching vectors in the rotating or stationary frame plane, based on the position of the output voltage vector in each sector of the space vector sectors. The mathematical model of SVPWM inverter is given as seen on (Eqs. (12) and (13)), where n represents the number of the space vector sectors.

$$T_a = \frac{\sqrt{3}T_z V_{ref}}{V_{dc}} * \left(\sin\left(\frac{n\pi}{3} - \alpha\right)\right) \tag{12}$$

$$T_b = \frac{\sqrt{3}T_z V_{ref}}{V_{dc}} \left(\sin\left(\alpha - \frac{n-1}{3}\pi\right)\right) \tag{13}$$

2.3 Mathematical model of stationary field transformation

The transformation from the mechanical model has completed by the usage of the d-q transformation, which is used for a vector manipulate approach of the synchronous motor machine. The base at the concept which is the windings of the stator are disbursed a d-q version is a powerful tool for simulation of all AC machines such as the SynRM [6, 7, 16]. When Three-segment balanced and altered windings and symmetry to two-segment Equation Equilibrium windings deliver rotating magnetic discipline speed Φ and cost are equatorial, the three-section windings are Equational with the two-segment windings. The d-q transformation is well-balanced three-phase V_d,V_b andV_c into balanced two-phase V_d and V_q as shown in **Figure 4**.

The transformation matrix "T" to transfer voltage or current vector from abc reference frame into dq reference frame as seen on (Eq. (14)):

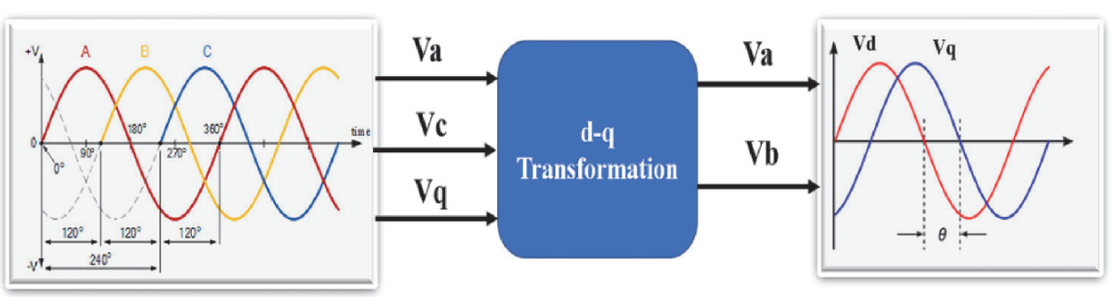

Figure 4.
The direct and quadratic voltage transformation.

$$\begin{bmatrix} V_d \\ V_q \\ V_o \end{bmatrix} = \mathbf{T} \begin{bmatrix} V_a \\ V_b \\ V_c \end{bmatrix} \tag{14}$$

The transformation matrix can be used in synchronous frame as explained in (Eqs. (15) and (16)),

$$\mathbf{T} = \sqrt{\frac{2}{3}} \begin{bmatrix} 1 & \frac{-1}{2} & \frac{-1}{2} \\ 0 & \frac{\sqrt{3}}{2} & \frac{-\sqrt{3}}{2} \\ \frac{1}{\sqrt{2}} & \frac{1}{\sqrt{2}} & \frac{1}{\sqrt{2}} \end{bmatrix} \tag{15}$$

$$\mathbf{T}^{-1} = \sqrt{\frac{2}{3}} \begin{bmatrix} 1 & 0 & \frac{1}{\sqrt{2}} \\ \frac{-1}{2} & \frac{\sqrt{3}}{2} & \frac{1}{\sqrt{2}} \\ \frac{-1}{2} & \frac{-\sqrt{3}}{2} & \frac{1}{\sqrt{2}} \end{bmatrix} \tag{16}$$

Where T^{-1} represents the inverse transformation matrix.

$$\begin{bmatrix} V_d \\ V_q \end{bmatrix} = \sqrt{\frac{2}{3}} \begin{bmatrix} 1 & \frac{-1}{2} & \frac{-1}{2} \\ 0 & \frac{\sqrt{3}}{2} & \frac{-\sqrt{3}}{2} \end{bmatrix} \begin{bmatrix} V_a \\ V_b \\ V_c \end{bmatrix} \tag{17}$$

The zero-axis voltage is neglected, and the power is the same in both the three phase and the two-phase transformation as seen on (Eq. (17)).

3. Motor control

3.1 Traditional cascade PID controller

Traditional PID controllers are considered the most largely used controllers in the control-process industry because of their simple structure and easy parameter settlement. The major cause of user feedback is a very substation in systems is to be able to attain a set-point regardless of disturbances, noise, or any variation in characteristics [5–16, 25]. A PID controller determines an "error" value as the difference between an obtained process variable and a reference setpoint. **Figure 5** shows the general cascade control system scheme. The controller tries to make the error signal as small as possible by manipulating the process control inputs. The calculation "algorithm" of the PID controller contains three separate constant parameters, and it is mainly called the proportional, integral, and derivative values [5–16, 29]. The differential equation of a PID controller is given by (Eq. (18)).

$$u(t) = k_p e(t) + k_i \int e(t)dt + k_d \frac{d}{dt} e(t) \tag{18}$$

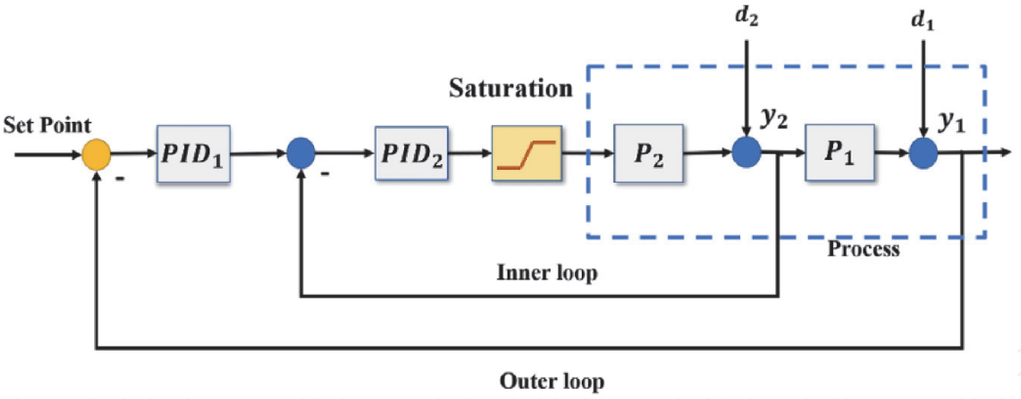

Figure 5.
The General Cascade control system scheme.

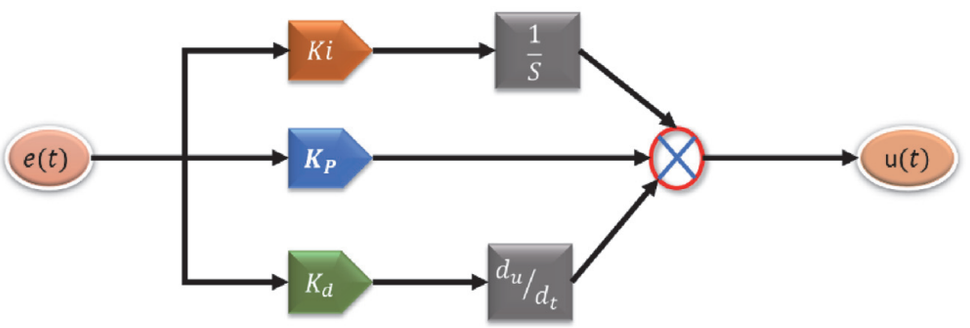

Figure 6.
Traditional PID controller.

Response parameter	Rise time	Overshoot	Settling time	Steady-state error
K_P	Decrease	Increase	Small change	Decrease
K_I	Decrease	Increase	Increase	Eliminate
K_d	Small change	Decrease	Decrease	Small change

Table 2.
The characteristics of the tradition controller.

Moreover, the transfer function is given by (Eq. (19)).

$$G_{PID}(s) = k_p + \frac{k_i}{S} + S.k_d \tag{19}$$

Figure 6 shows the block diagram with the parameters of the PID controller. The response to the error is connected to the proportional value, the sum of mistakes that were recent are the integral's assignment to determined and the reaction is being represented by the derivative to the rate at which the error has been shifting. The controller parameters K_P, K_I and K_d on traditional closed-loop systems as shown in **Table 2** give comprehensive effects of each parameter, in some control processing it may require only one or two parameters to present a suitable control system. Setting other parameters to zero is the method for correcting the PID controller to two or one activity. A PID controller will be named a PI, PD, P or I controller when neglecting one of the respective control actions [5, 6, 12]. PI controllers are common, since the activity is sensitive to sound change, whereas if there is absolutely no term that is integral the system may be avoided by it from reaching its target value due to the control activity [11–16].

3.2 Cascade control system

The procedures have more than one variable or factor at the output. That should be controlled is well known as a term multivariable or MIMO processes. Interactions usually exist or occasionally do not exist between the control loops of multivariable processes, which is famed by problems in control when compared with the Single Input/Single Output (SISO) control processes. Lead–lag compensators are utilized to provide a combines performance involving both lead and lag compensator and utilized as another phase following PI and PID controllers which allow the machine to have stabilized functionality [5, 6, 12, 26]. PI controller was utilized to control the guide axis current. This sort of control procedure is shown in **Figure 7**. The disadvantages of the type of control an ambiguity of control engineers' power SISO PID controller, flexibility for both interaction adjudication and compare it with overall multivariable control it is a couple of strong tools for its layout [6–9]. Therefore, there is one easy method to tune a multi-loop PID controller by tuning each loop one by induvial work, and completely discarding the loop connections and that is carried out by the (i) loop of cascade controller for the plant move. Then re-tuning all the loops together so the general system has stable functionality and supplies a suitable load disturbance response [5, 6, 12, 26–29].

3.3 Double-led compensation

The lead compensators are used to give advance phase margin, used in this chapter as a second stage after PID controller, and used to control quadrature axis current double-lead compensators to make the system have advanced stabilized performance because it is considered a cascaded lead compensator [6, 7–12]. The double lead compensator gives double of the phase advance that a simple lead compensator that gives. The double lead compensator mathematical description can be given in (Eq. (20)). The lead compensator is utilized to control the quadrature axis present of this SynRM.

$$G_{pd}(s) = K_p \frac{\left(1 + s/\omega_z\right)^2}{\left(1 + s/\omega_p\right)^2} \tag{20}$$

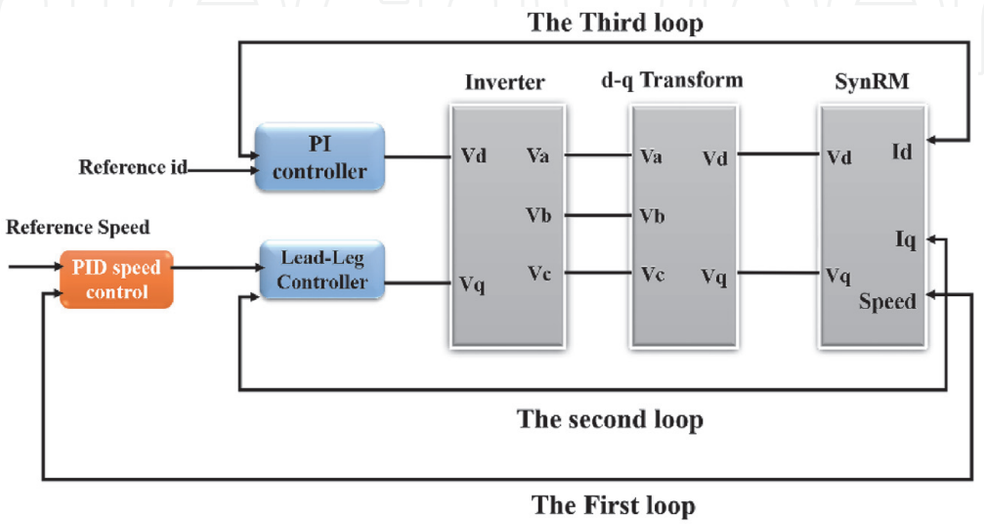

Figure 7.
Cascade controller block diagram.

3.4 Practical swam optimization tuning PID controller parameter

The Particle Swarm Optimization (PSO) is a public rely on computational approaches that the primary concept came in the simulation of social behavior "social-psychological methods" fish instruction, bird flocking and swarm concept. PSO was initially designed and evolved by Eberhart and Kennedy [4, 6, 12] This concept was designed to be effective in solving problems exhibiting non-linearity and non-differentiability. The scheme is obtained from research on swarms such as fish Instruction and bird flocking. Accommodation to the results of research for a flock of birds finds that bird's food by flocking (not by everyone). Instead of using the evolutionary proses such as mutation and crossover that been used for algorithm manipulation. In the PSO algorithm, none of these presses are used, the dynamics of the population simulates a "fish flocks" attitude, where sociably sharing of information takes a major part of work and individuals can profit from discovering and former experience of all the other escorts during the food searching process [4]. The fitness function is cast to maximize the constraints domain or to minimize the preference constraints. The most common performance criteria that depend on the error criterion are Integrated Absolute Error (IAE), Integrated of Time Weight Square Error (ITSE) and integrated of Square Error (ISE) which can be calculated analytically in the frequency domain. The criteria selection depends on the system and the controller [5, 6, 12–16]. In this chapter the fitness functions are used depend on the ISE criterion and the overshoot $M_p$criterion as seen on (Eqs. (21)–(24)).

$$\text{Fitness function} = \min(\text{ISE}) + \min(M_p) \tag{21}$$

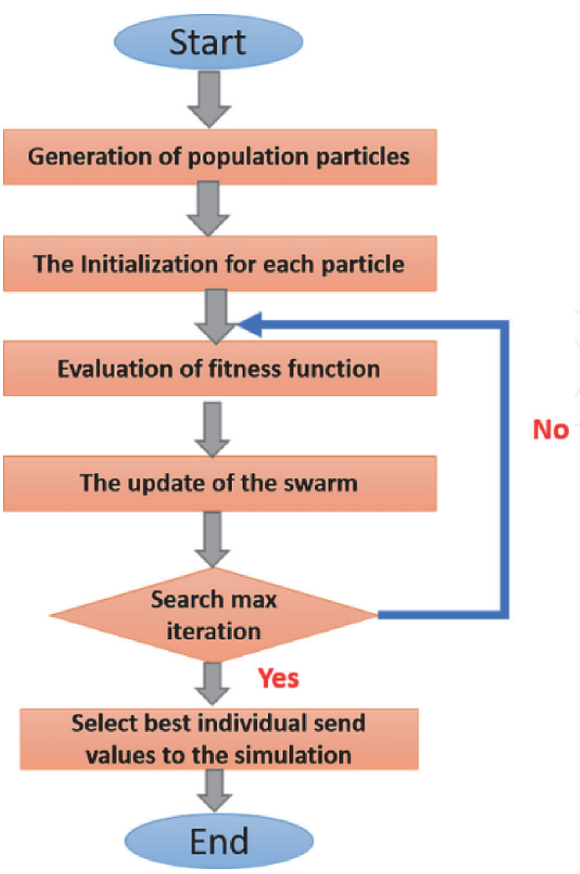

Figure 8.
The PSO algorithm steps.

$$ISE = \int e^2(t)dt \tag{22}$$

$$M_p = \max(n) - (n_{ref}) \tag{23}$$

$$e(i) = D(i) - y(i) \tag{24}$$

The $v_i(t)$ and $x_i(t)$ updating for each particle in the swarm are done depending on (Eqs. (25) and (26)). Then starting the main loop and the fitness function are calculated to update the positions of particles. If the new value is better than the quondam I_{best}, the new value is set to I_{best} . In the same way, g_{best} value is also updated like the I_{best}. The velocity of each agent can be updated by (Eq. (25)).

$$v_i^{k+1} = w * v_i^k + c_1 * R_1 * \left(lbest_i - x_i^k\right) + c_2 * R_2 * \left(gbest_i - x_i^k\right) \tag{25}$$

Moreover, the current position can be updated by (Eq. (26)):

$$x_i^{k+1} = x_i^k + v_i^{k+1} \tag{26}$$

$$w = w_{max} - \frac{(w_{max} - w_{min})}{iter_{max}} \tag{27}$$

The diagram below explains the order of PSO processes and steps that were adopted and implemented in this design as expend in **Figure 8**.

4. The design of the propulsion EV system

The proposed system is called the Multi-Converter/Multi-Machine System (MCMMS) which consists of two SynRM that drive the two rear wheels of PEV [6, 7, 12, 13]. The linear speed of the vehicle is controlled by an EDC which gives the reference speed for each driving wheel which depends on the driver reference speed and the steering angle. Different road conditions have been applied by the Drive cycle topology to test the stability of the EV under the EDC controller. The SynRM speed is controlled by using a PID controller and the PSO algorithm has been used as an optimization technique to find the optimal PID parameter to enhance the drive system performance [2–4, 24]. The VSSVI has been used to transform the DC voltage source to three-stage AC voltage [1, 2]. The EV system has tested implemented in the Matlab/Simulink environment. Moreover, the mechanical load that reflects the street state of the vehicle each one of these elements has been displayed in **Figure 9**. Which shows a succinct description to the suggested system the two-wheel driveway process is perceptible to everyone to grantee the equilibrium of the EV on various road state [1–12].

The inner construction system for this type of EV has controlled by an EDC system that ensures the robustness of the motor vehicle [1–5]. In addition, the propulsion electric vehicle system process has referred to as a MCMMS [18, 22]. Moreover, the pure-electric-vehicle is much simplified and like the traditional mechanical vehicle in the work way, because of slipping issues from the curvature or slope “inclined” angle roads [16, 17, 23].

4.1 The electronic differential controller (EDC)

The EDC is an electronic device that guarantees deliver a maximum value of the torque and control both driving wheels, so each wheel may turn at different speed

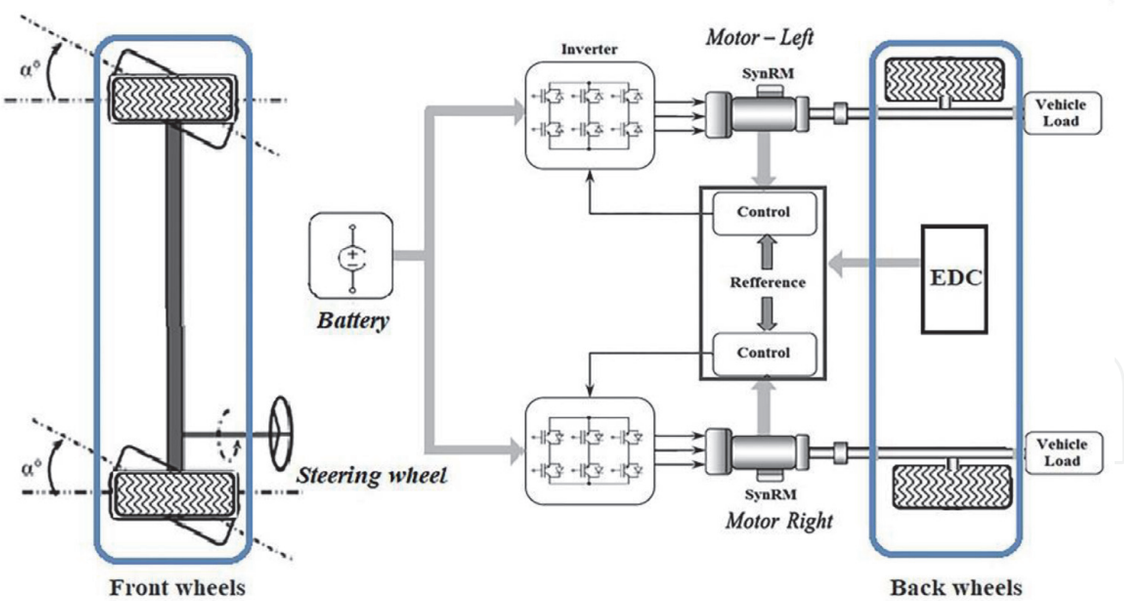

Figure 9.
Propulsion system control of the EV.

rates in virtually any curve or precisely the exact same rate of speed in the right line road. According to the road condition and especially the steering angle control of the vehicle, the electric power is distributed by EDC to each electric motor [4, 9–12, 27]. In addition, the most critical beholding in the plan of the EVs will be to make sure that the EV is secure when cornering' and under slippery road' conditions [9, 14, 15]. **Figure 10** shows the EV structure pushed at a curve road. The calculation of the speed rate of the vehicle is a task of EDC work, also is based mostly on; the driver, vehicle dimension and street condition. The linear speed rate as well as the steering angle that has awarded by the driver, which implies that both inputs regarded as the input reference to the EV system [9, 17–20, 27–30].

At the beginning of the vehicle's turn in the curve road, the driver utilizes the curve steering angle to the steering wheel to drive and control the vehicle. In this case, the EDC reacted quickly and calculate the benchmark speed of each wheel ought to be operating that appropriately and synchronous to ensure the equilibrium of the EV functionality within the curve street by increasing the speed rate of an outer motor and diminishing the speed rate of the Internal motor [4, 12, 17]. The mathematical model of this EDC signifies via (Eqs. (28) and (29)).

$$V_L = \omega_v \left(R + \frac{d_\omega}{2} \right) \tag{28}$$

$$V_R = \omega_v \left(R - \frac{d_\omega}{2} \right) \tag{29}$$

The curve road can be determined as (Eq. (30)).

$$R = \frac{L_\omega}{\tan \delta} \tag{30}$$

Moreover, the angular speed rate in a curve road for both wheels can obtain by the following in (Eqs. (31) and (32)) bellow:

$$\omega_L = \frac{L_\omega + \frac{d_\omega}{2} \tan \delta}{L_\omega} \omega_v \tag{31}$$

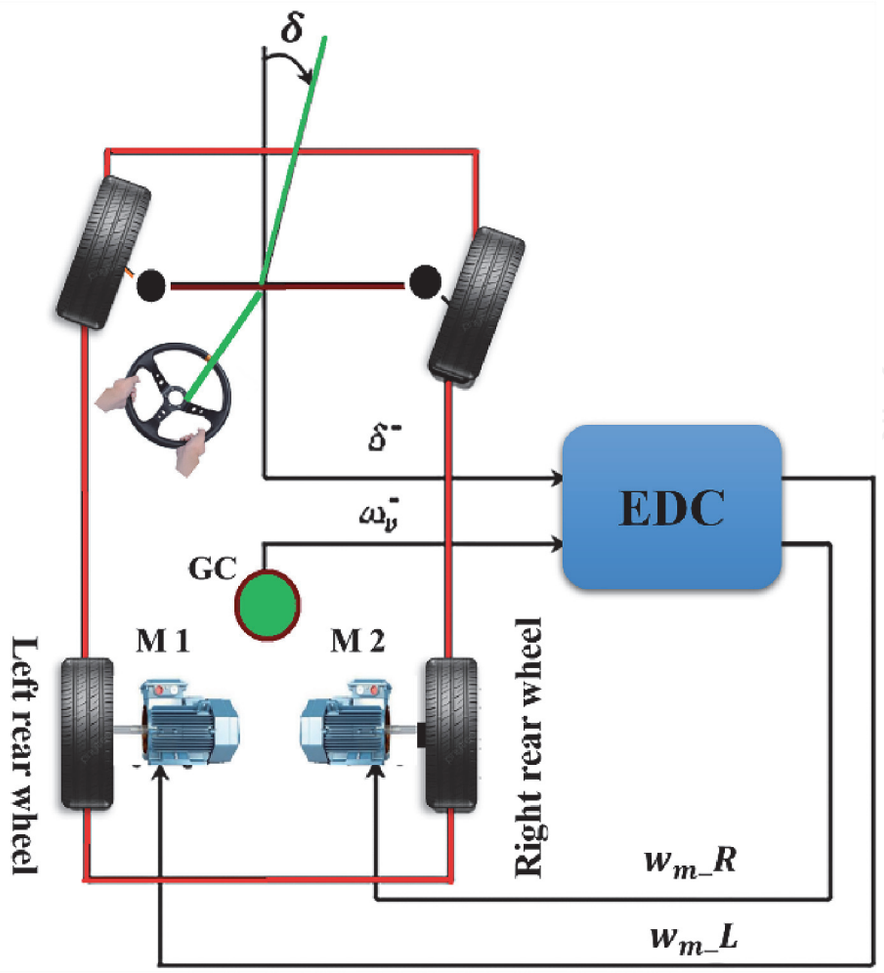

Figure 10.
The input and output of the EDC on the curve road.

$$\omega_R = \frac{L_\omega - \frac{d_\omega}{2}\tan\delta}{L_\omega}\omega_v \tag{32}$$

The difference in Rate between both of them (the left and right wheels) could be write as (Eq. (33)) bellow:

$$\Delta\omega = \omega_L - \omega_R = \frac{d_\omega . \tan\delta}{L_\omega}\omega_v \tag{33}$$

Besides, the mention of the speed rate for both Wheel engine can be described as (Eqs. (34) and (35)) bellow:

$$\omega_{Lr} = \omega_v + \frac{\Delta\omega}{2} \tag{34}$$

$$\omega_{Rr} = \omega_v - \frac{\Delta\omega}{2} \tag{35}$$

The Terms of the angle (δ) condition in both of straight or curve road are:

- First term: Turn right→ (δ > 0)
- Second term: straight ahead→ (δ = 0)
- Third term: Turn left→ (δ < 0)

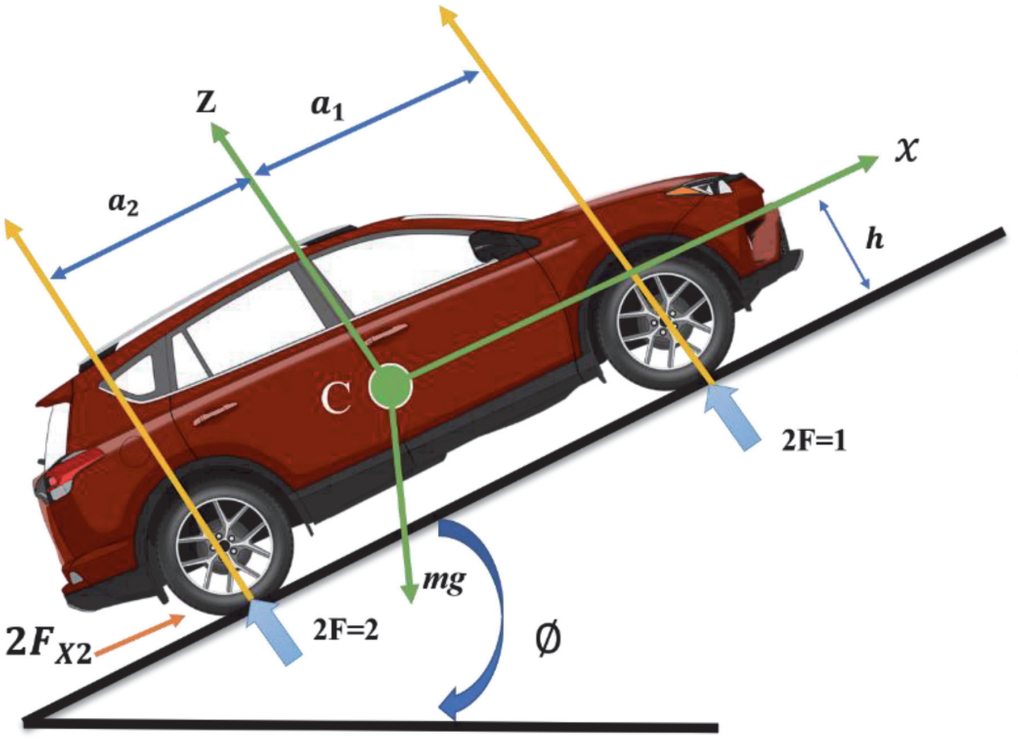

Figure 11.
The effective forces of the EV in an inclined road.

4.2 The resistive forces of EV

Typically, the EV regarded as a succession of heaps that described by numerous forces mainly or resistive torque. Anyway, the forces may include three components, which will be the rolling resistance, the aerodynamic resistance along with also the pitch "incline" resistance [4]. The forces acting in an EV moving across a likely road is displayed in **Figure 11**.

The resistive forces which influenced on the EV are described as seen on (Eq. (36)). And the effective rolling resistance can be described as seen on (Eq. (37)) [31].

$$T_r = T_{aero} + T_{slope} + T_{tire} \tag{36}$$

$$T_{tire} = mgf_r \tag{37}$$

The force of the aerodynamic resistance can be explained in (Eq. (38)):

$$T_{aero} = 1/2\rho_{air}A_fC_dV^2 \tag{38}$$

Moreover, the force of the slope "incline" resistance describes in (Eq. (39)):

$$T_{slope} = mgsin\beta \tag{39}$$

5. Simulation and results

5.1 Simulation and results of cascade-PI and lead-lag-controller

A single cascade controller with several control loops has been used in industrial processes. Since it provides an advantage in terms of ease of execution and the

ability to manually set the parameter of this managed kind. Furthermore, as compared to overall multivariable control, which has a few robust tools for its architecture, this control category has a high demand for interaction versatility modification. In this case, a system engineering team manually tunes the SISO for the PID controller to complete the control loop for this form of control. Even so, there is a single basic strategy for tuning a multi-loop PID control, which is to tune control loops step by step while refusing loop interaction completely. Furthermore, the install switch operation has been carried out by setting the I loop of the PID control. The machine would have steady functionality and a suitable load disruption response if the full loops are re-tuned together. To restrain the quadrature-axis (q) that exists in the SynRM, the lead–lag compensator was proposed.

Simultaneously, the procedure is depended on **Figure 6** that represents the SynRM cascaded control system. **Figure 12** explains the simulation for the cascaded PI controller model with the lead–lag compensator. **Table 3** reveals the cascaded controller parameters value of the cascaded controller system that has utilized by a strategy known as "trial and error". The **Figures 13–18** reveals the SynRM speed rate and torque due to different working condition.

5.2 Simulation and results of cascade-PI, PID and lead-lag-controller

The PI controller at the speed rate control has substituted via PID controller, which the metering activity gives to improve the motor speed and torque activity. As shown in **Table 4**, the cascaded PI and PID control parameters have utilized via trial-error strategy. Besides, **Figure 19** shows the Matlab/Simulink program has employed to simulate the PI and PID-cascaded controller. The **Figures 20–25** reveals the SynRM speed rate and the torque due to several working conditions.

5.3 Simulink and results for the cascaded controller with PSO

The cascaded PID, PI, and lead–lag compensator were used to simulate the SynRM model based on the results of the PSO algorithm discovered by using the

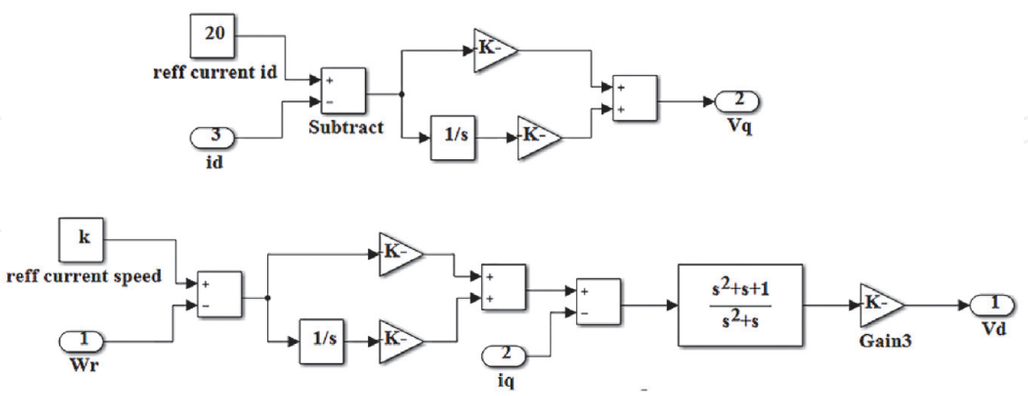

Figure 12.
Simulink model for cascade-PI and lead- lag controller.

The type of controller	Speed		Quadratic axis current		
The Parameters	K_P	K_I	K_3	K_P	K_I
The Result value	60.245	17.672	22	2130	9.8

Table 3.
The parameters and values of the cascade controller.

DOI: http://dx.doi.org/10.5772/intechopen.98873

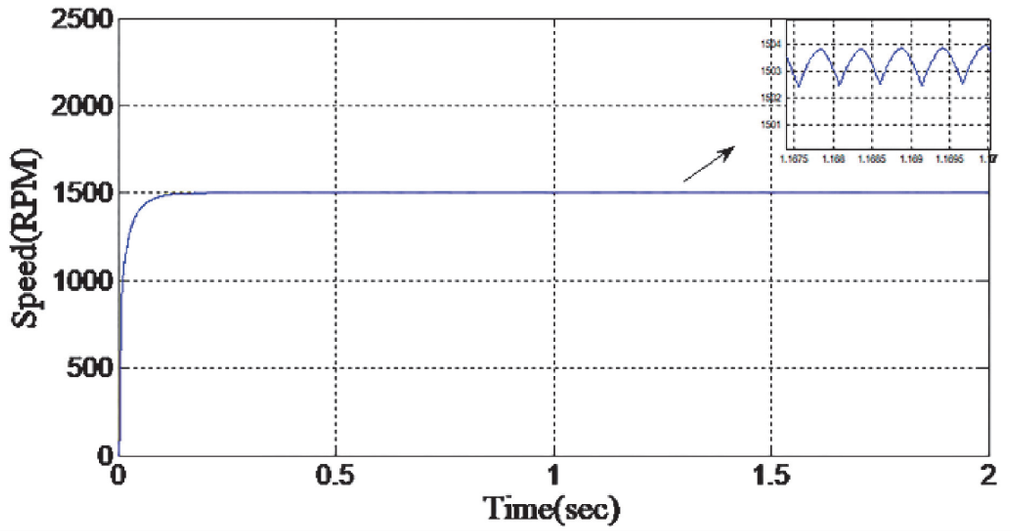

Figure 13.
SynRM speed control at 1500 rpm with no load condition.

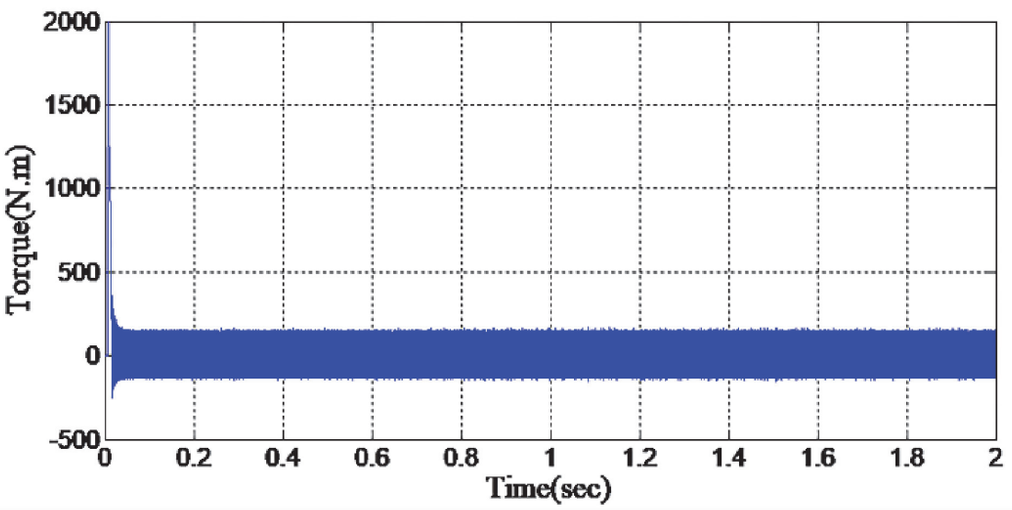

Figure 14.
The SynRM torque control at1500 rpm with no load condition.

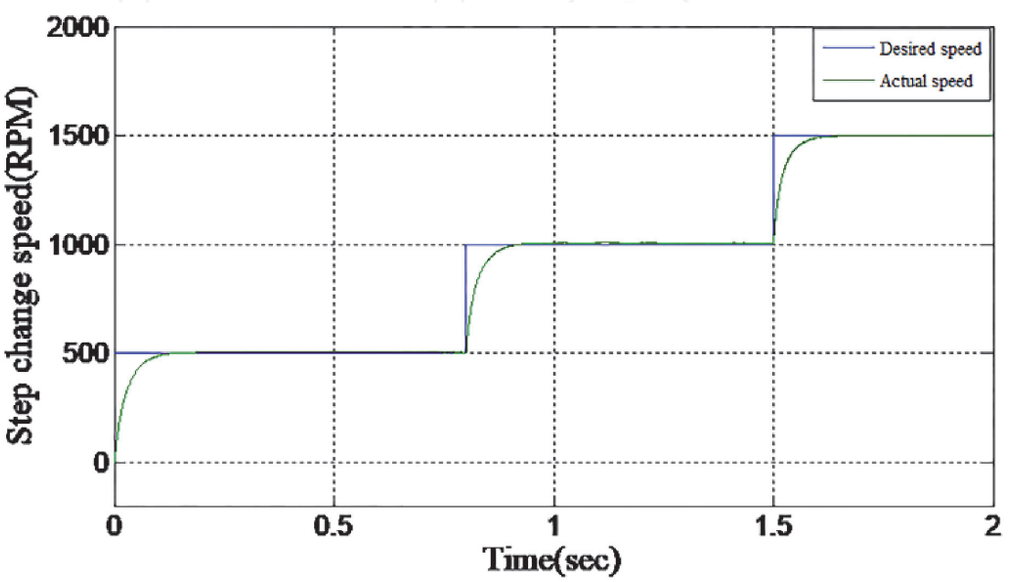

Figure 15.
The SynRM speed control at steps of speed.

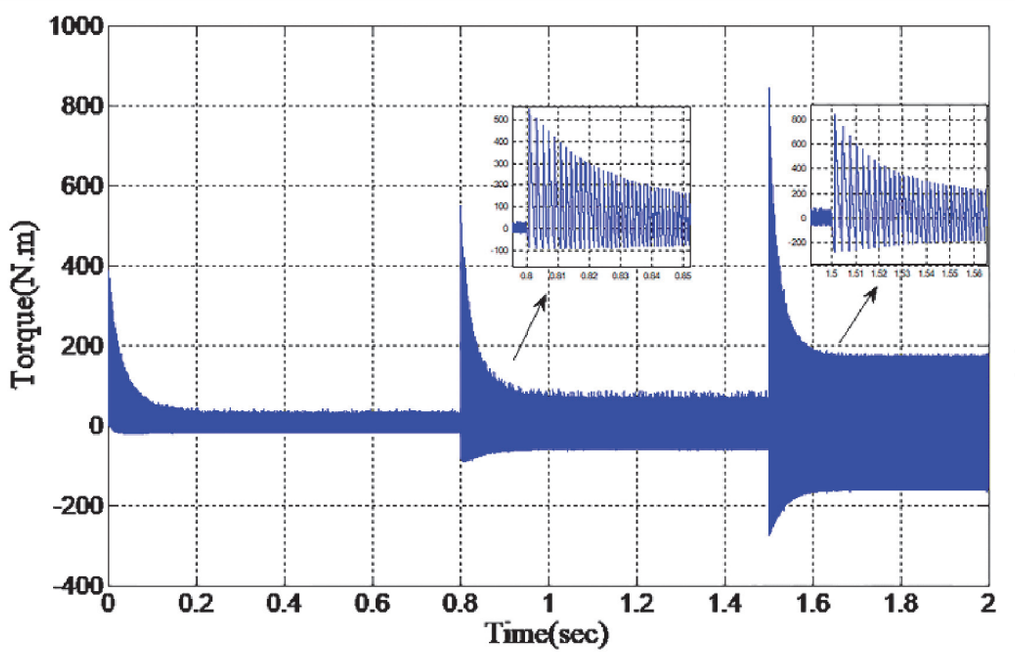

Figure 16.
The SynRM torque control at steps of speed.

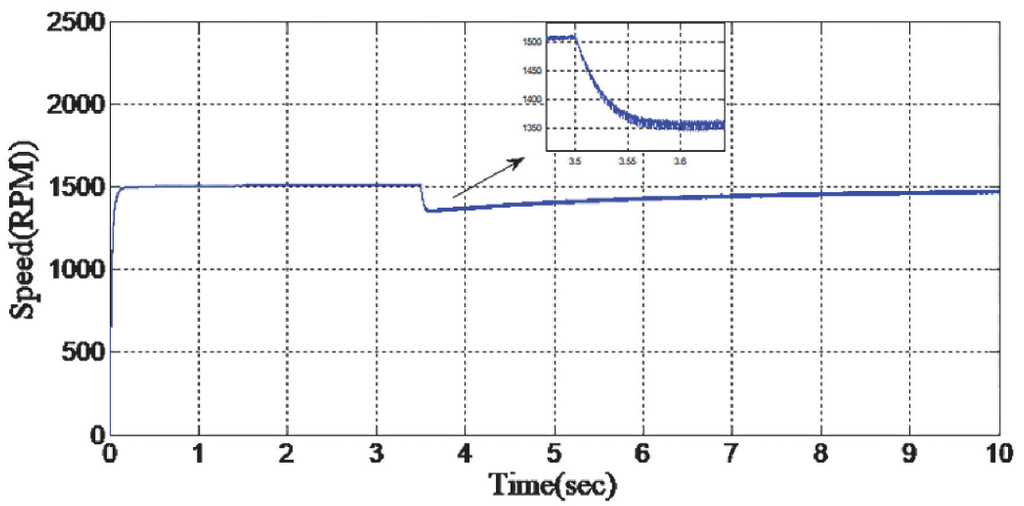

Figure 17.
The SynRM speed control with 1500 rpm *and 50* N.m *of load applied at 3.5 second.*

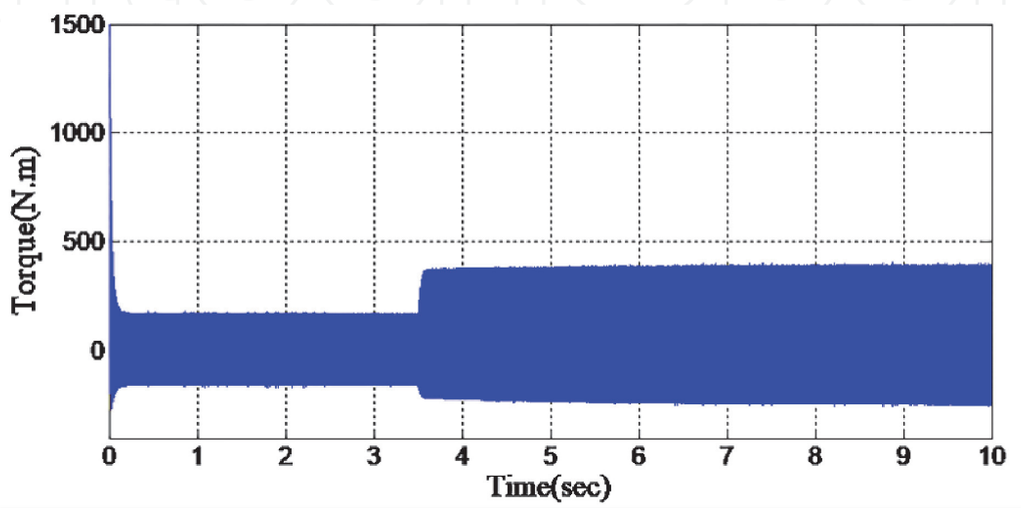

Figure 18.
The SynRM torque control at 1500 rpm with 50 N.m of load applied at 3.5 second.

'The type-of controller'		Speed-		Quadratic*Axis*Current		
The parameter	K_{P-}	K_{I-}	K_{d-}	K_{3-}	K_{P-}	K_{I-}
The value	40	10	1	22	1200	10

Table 4.
Manually tuned of the cascade controller.

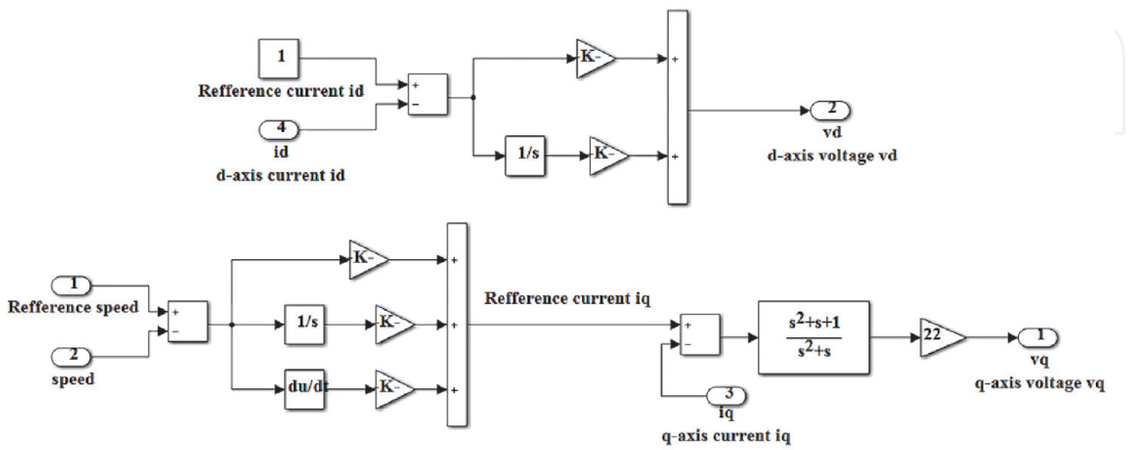

Figure 19.
Simulink model for PI, PID and lead–lag controllers.

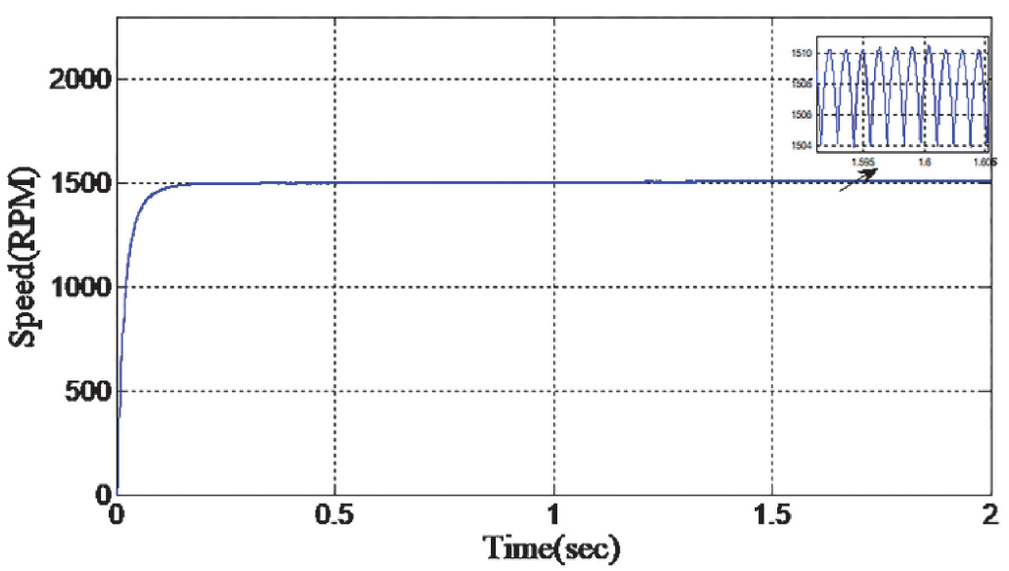

Figure 20.
The SynRM speed control at 1500 rpm with no load condition.

Simulink method with the PSO algorithm. The Simulink findings show characteristics and feature the PSO algorithm, which offers optimal PID, PI, and lead–lag-compensator parameter values to improve system functionality as shown in **Table 5**. Besides, **Table 6** shows the parameters of the PSO strategy tuned in cascade controller. **Figure 26** displays the technique parameters PID and PSO. Furthermore, the **Figures 27–32** show the SynRM speed control and torque control from PSO algorithm parameters of the cascaded control with approximately 50 integrations.

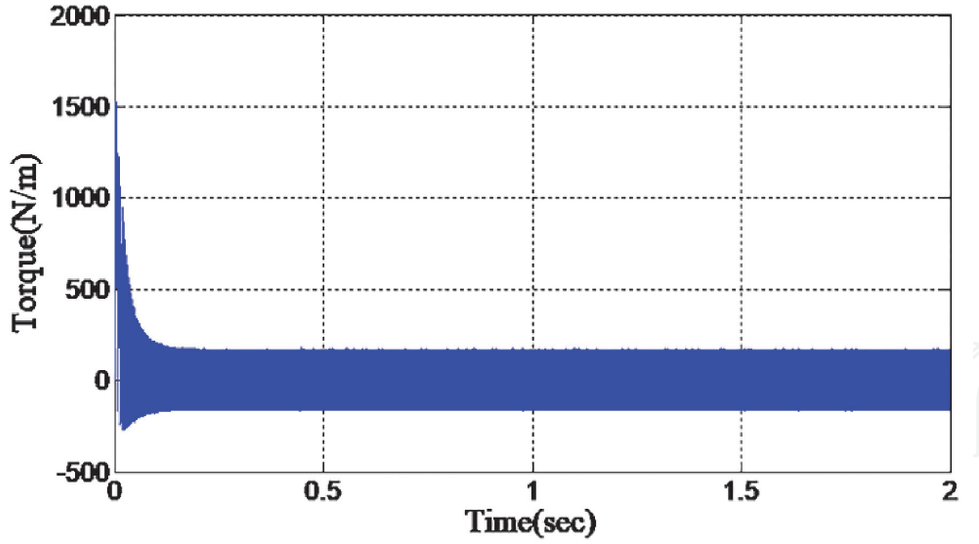

Figure 21.
The SynRM torque control at 1500 rpm with no load condition.

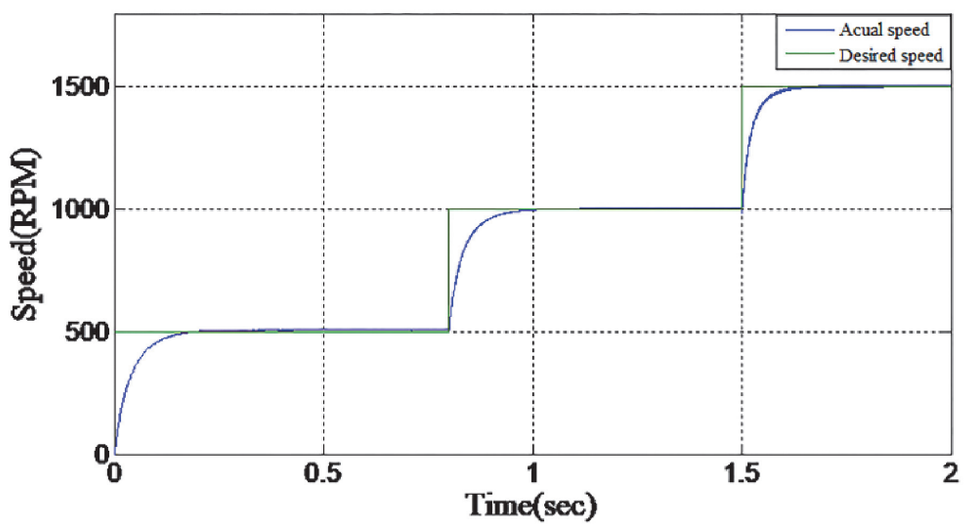

Figure 22.
The SynRM speed control with steps of speed.

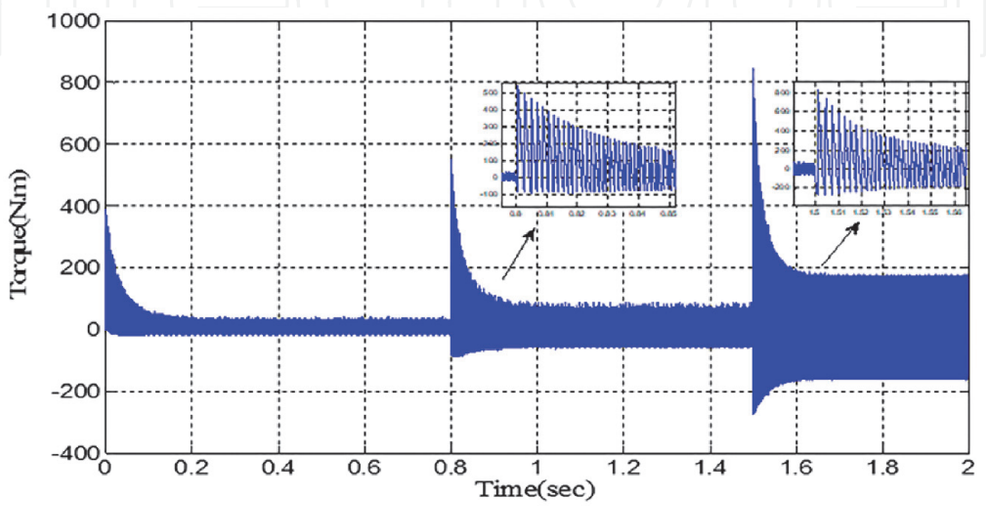

Figure 23.
The SynRM torque control with steps of speed.

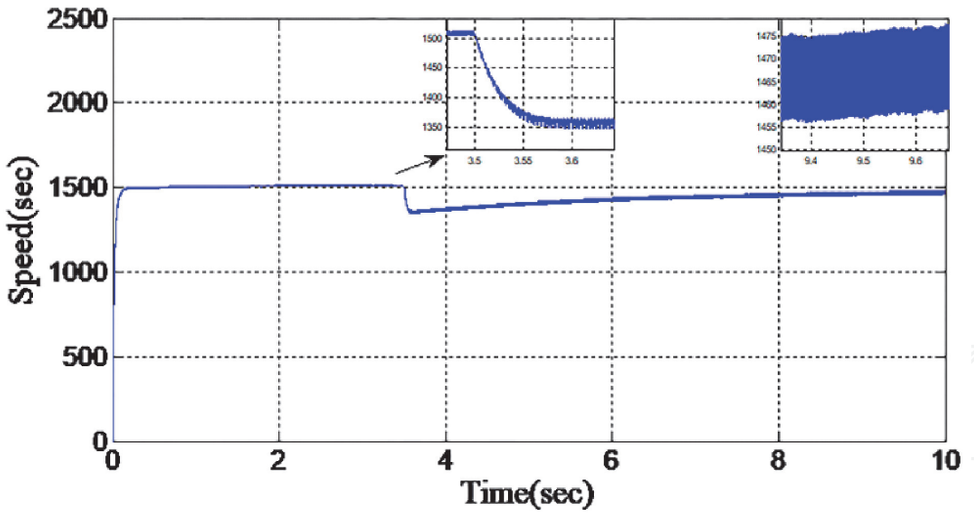

Figure 24.
The SynRM speed control with 1500 rpm and 50 N.m step of load applied at 3.5 second.

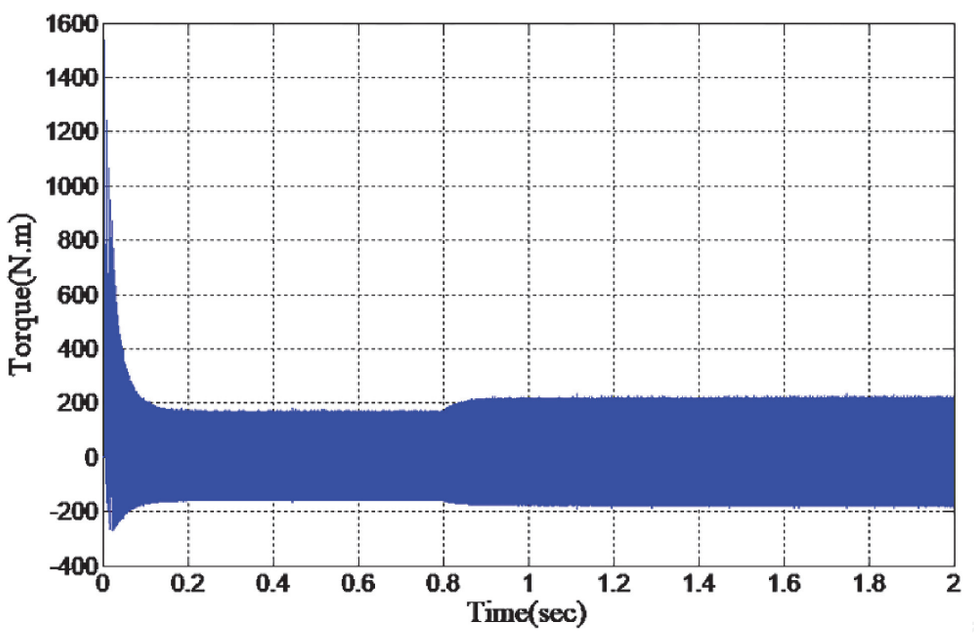

Figure 25.
The SynRM torque control with 1500 rpm *and 50* N.m *step of load applied at 3.5 second.*

The PSO parameters	The value
The Size of the swarm.	50
Maximum iteration number.	50
The Swarm Dimension.	16
C_1 parameter.	1.3
C_2 parameter.	1.3
$W_{max.}$	0.8
$W_{min.}$	0.3

Table 5.
The characteristics of PSO algorithm.

The type of controller	Speed			Quadratic axis current		
Parameter	K_P	K_I	K_d	K_3	K_P	K_I
Value	200.64/	/8.8182/	/0.7914	/20.879	/2130	/9.8/

Table 6.
PSO strategy tuned.in-cascade-controller-parameters.

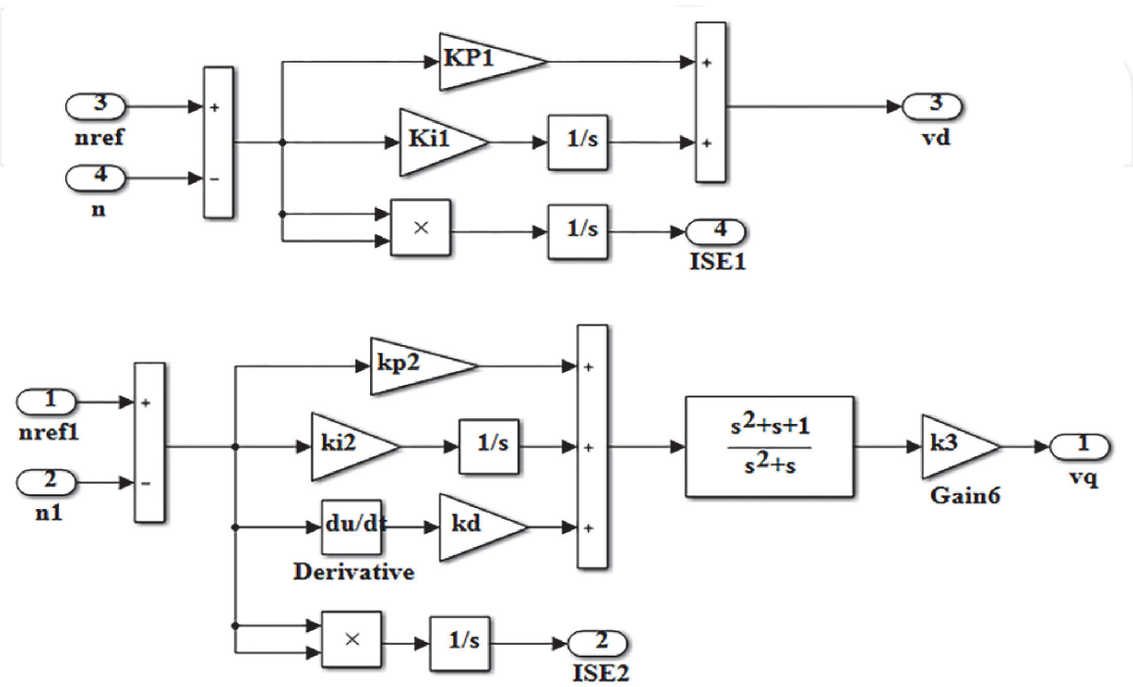

Figure 26.
Simulink for PSO fitness-function model.

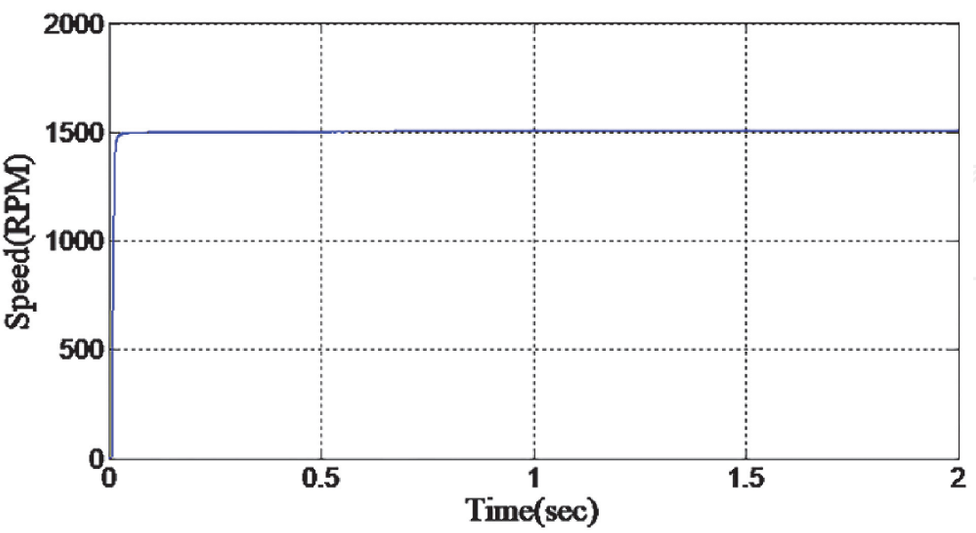

Figure 27.
The SynRM speed control with 1500 rpm and no-load condition.

5.4 Conclusion of SynRM controllers

The cascaded-PI and PID controls were used in conjunction with a lead–lag compensator to control the motor speed. Furthermore, the Simulink controls have been utilized to regulate the motor speed in a wide range and can provide adequate

DOI: http://dx.doi.org/10.5772/intechopen.98873

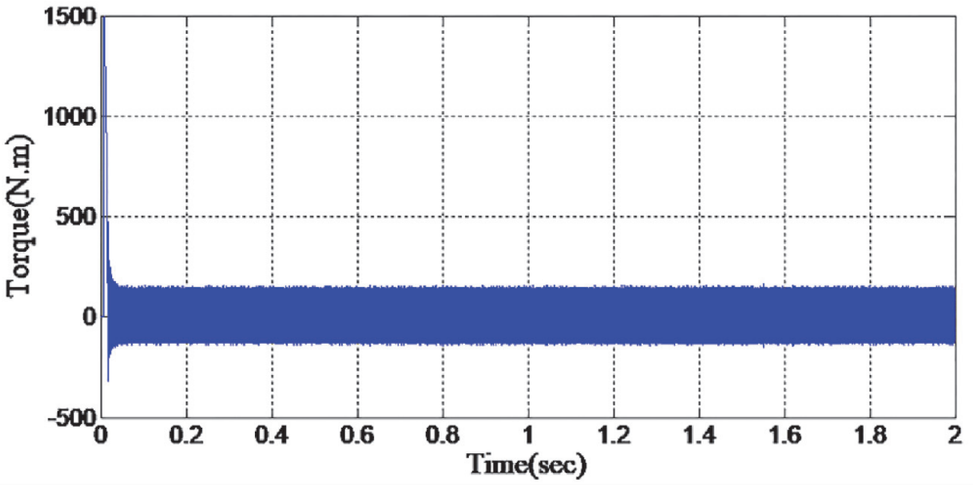

Figure 28.
The SynRM torque control with 1500 rpm with no load condition.

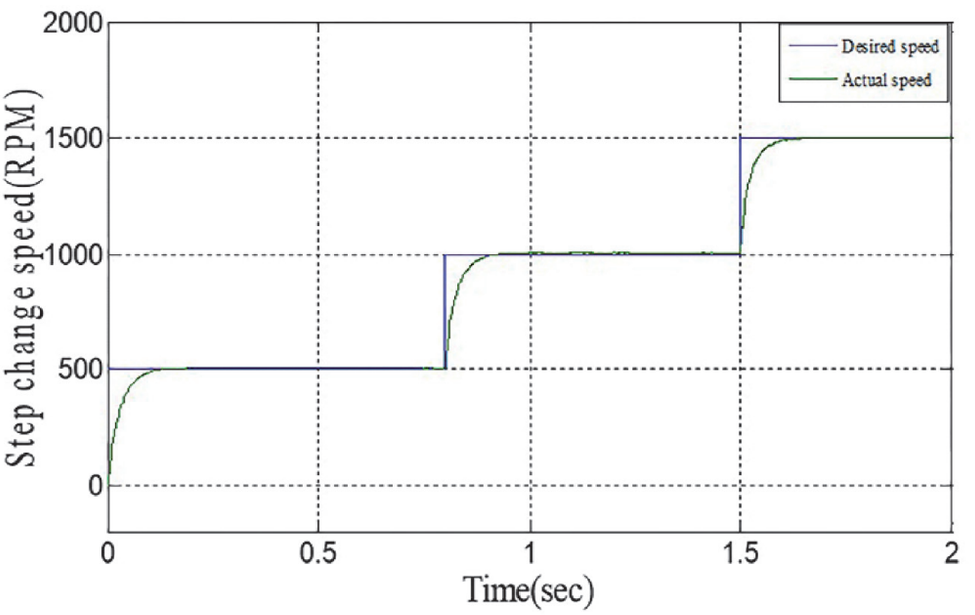

Figure 29.
The SynRM speed control with steps of speed.

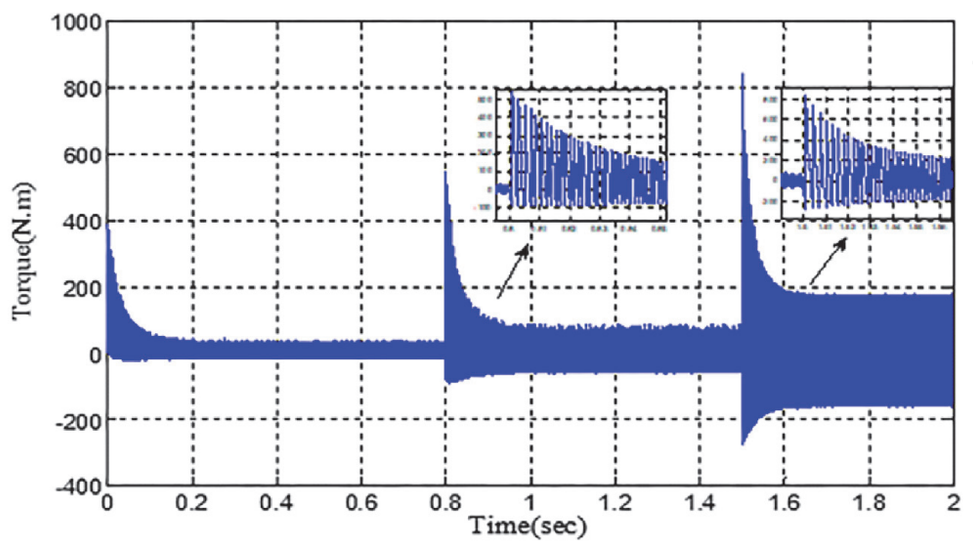

Figure 30.
The SynRM torque control with steps of speed.

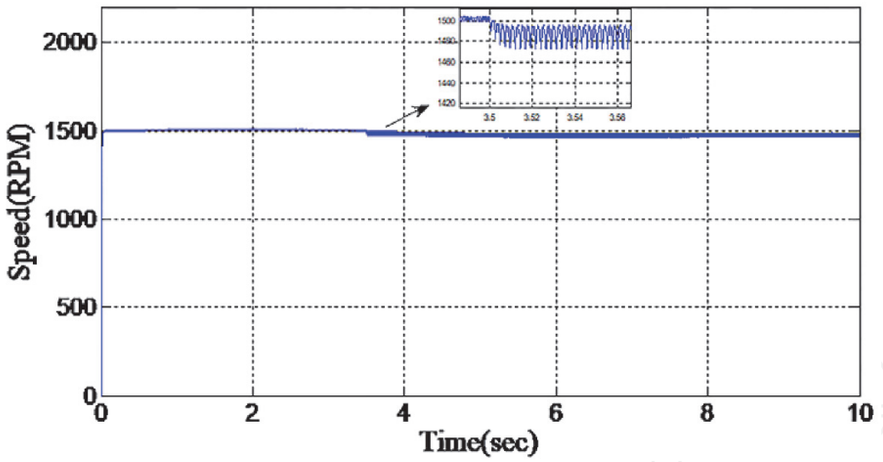

Figure 31.
The SynRM speed control with 1500 rpm and 50 N.m steps of load at 3.5 second.

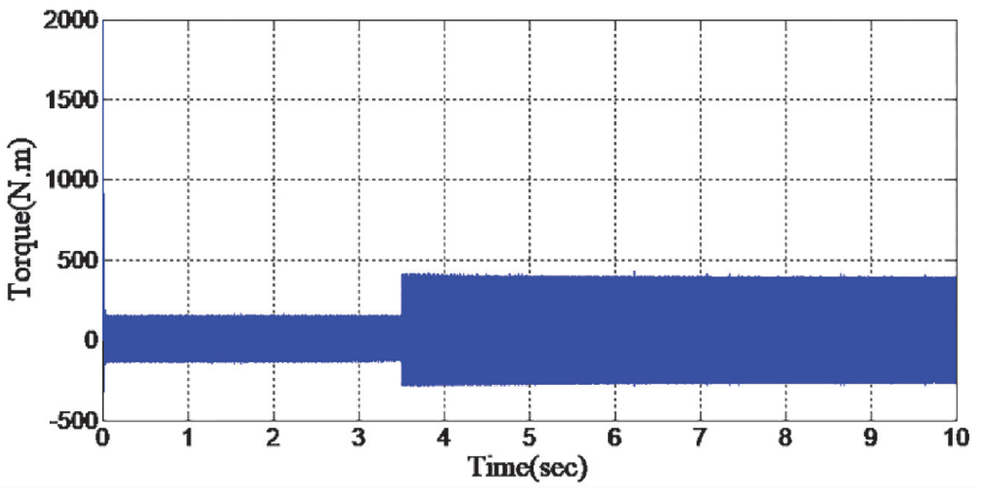

Figure 32.
The SynRM torque control with 1500 rpm and 50 N.m steps of load applied at 3.5 second.

speed and torque reaction or demonstrate their validity in regulating the motor speed rate in various operating conditions. Furthermore, the PSO algorithm simulated manipulating the parameters of their cascaded controls to achieve a more important output than traditional controllers. The simulation depicts the testing and study of each of the controller's structures under various circumstances. As a result, it is possible to infer that the proposed PSO strategy offers the best control parameters for improving system efficiency, especially in the loading state. The simulation depicts the testing and study of each of the controller's structures under various circumstances. As a result, it is possible to infer that the proposed PSO strategy offers the best control parameters for improving system efficiency, especially in the loading state.

6. The propulsion construction of EV

6.1 The simulation and design of the EV system

The simulation and design of the system have done via Matlab/Simulink depended on the above equations and the input parameters of these equations that have utilized in the design as showing in **Table 7** below:

DOI: http://dx.doi.org/10.5772/intechopen.98873

d_ω	**1.8 m**
R_w	0.23 m
f_r	0.02
m	710K_g
ρ_{air}	1.3K_g/m^3
A_f	2.8m^2
C_d	0.34

Table 7.
The design information of the EV.

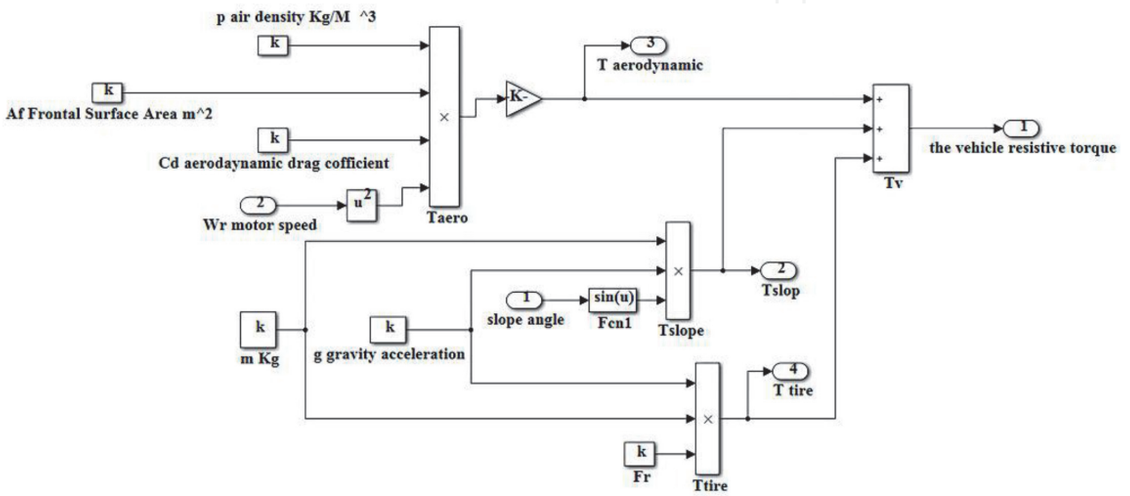

Figure 33.
Modeling and simulation of the resistive force.

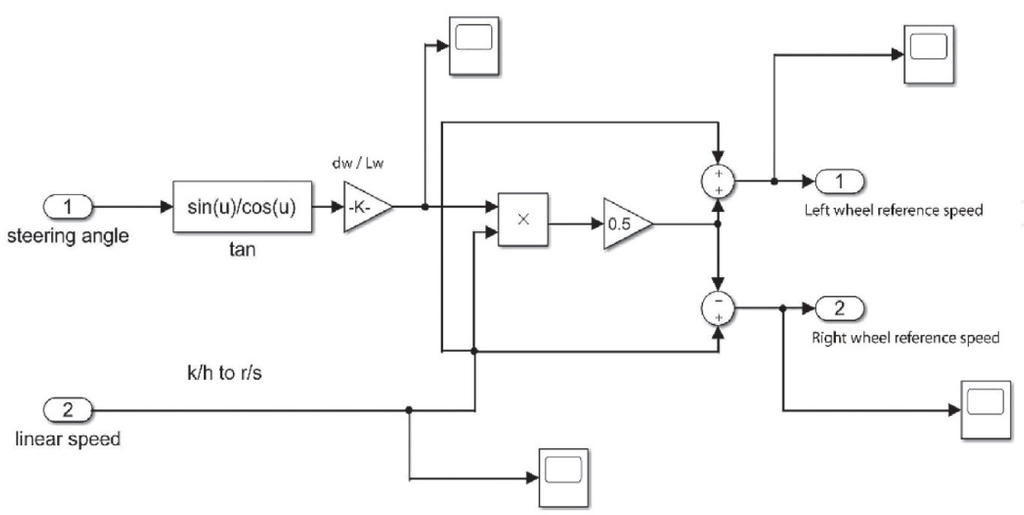

Figure 34.
The simulation diagram of the EDC system model.

6.2 Simulink model of the resistive torque in EV

The important task for the EDC is the distribution of the torque, where the resistive forces are dispersed evenly on both electric motors in the case of a straight road. Besides, the complete resistive of the torque is divided into two parts

"two-halves", which are each half distributed on a single motor. The torques supply is the EDC assignment. The modulation and simulation of the resistive force are represented in **Figure 33**.

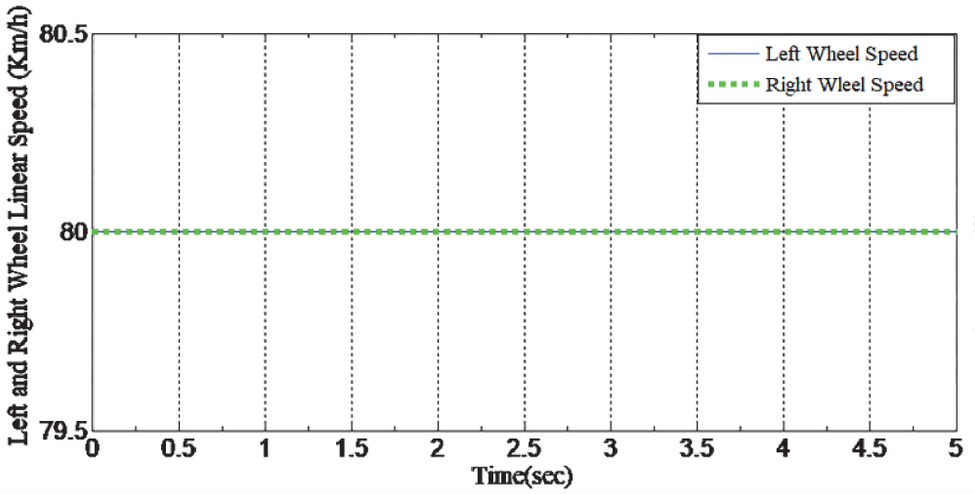

Figure 35.
The EV moving with 80 km/h speed rate at the straight road.

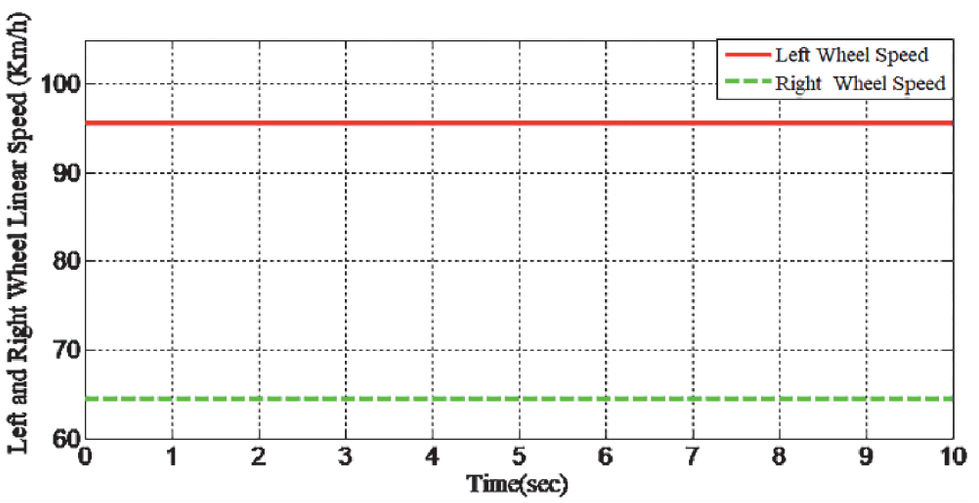

Figure 36.
The EV turn right with 80 km/h speed rate at the curve-road with +11-degree steering angle.

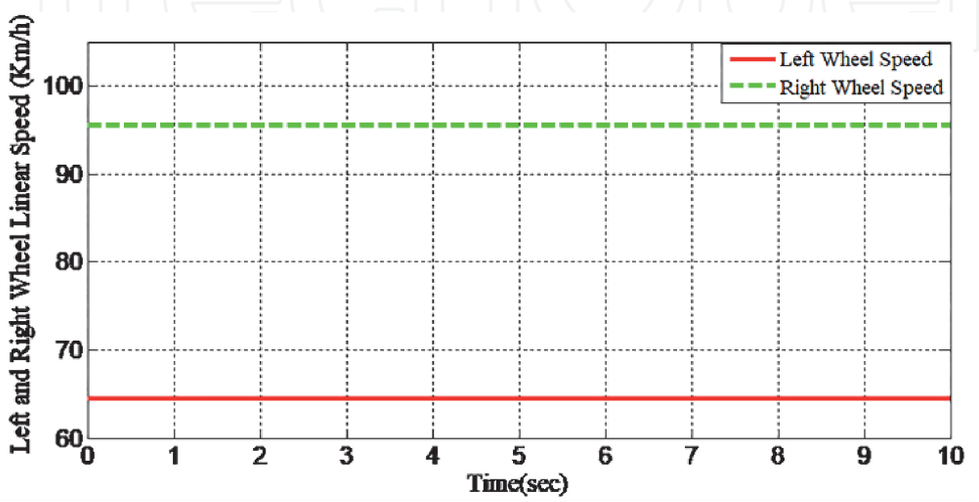

Figure 37.
The EV turn left with 80 km/h speed-rate at the curve-road with +11-degree steering angle.

6.3 The simulation and result of the EDC system

The simulation and result in this segment have applied using Matlab/Simulink software to describe and examine the validity of the EDC platform from the EV. Additionally, the simulation diagram of the EDC program version is displayed in **Figure 34**. The simulation model is designed based on the previously mentioned EDC equations. The simulation model represents two inputs to simulate the road conditions that the electric vehicle will travel: The first is the simulation of the inclined road with a different angle of inclination as needed in the simulations to test the vehicle on inclined roads. The second is the straight road, which has an angle of inclination of zero degrees. The model outputs represent the effect of different road conditions on the speed and stability of the electric vehicle, which is represented by the rear wheels of the vehicle that is connected to the EDC. Besides, the propulsion drive system layout at the EV includes two SynRMs that attached right on the wheels of the EV " right and left wheels" without decrease equipment, energy source signified by Lithium-Ion rechargeable battery power sours, EDC and VS-SVPWM inverter. In addition, **Figure 35** suggests the right road instance, where the two wheels in EV ought to be changed at precisely the exact same speed rate. Thus, once the EV turns directly from the curve street, the wheels proceed at a slow rate of speed when compared with the ideal wheels of the EV as shown in **Figure 36**. On the contrary, once the EV flip left from the curve street, the ideal wheels proceed at a higher rate of speed as compared with the wheels of their EV as shown in **Figure 37**.

6.4 The simulation result of driving cycles system

The EV **moving at 80 km/h of speed** as shown in **Figure 38** with comprise three stages. Moreover, the supply of this resistive force which impacts on the EV in these stages of the simulation differs from one point to another.

The supply of this resistive force that affects the EV in these stages of the simulation is somewhat different from one point to other. These stages are described as the points below:

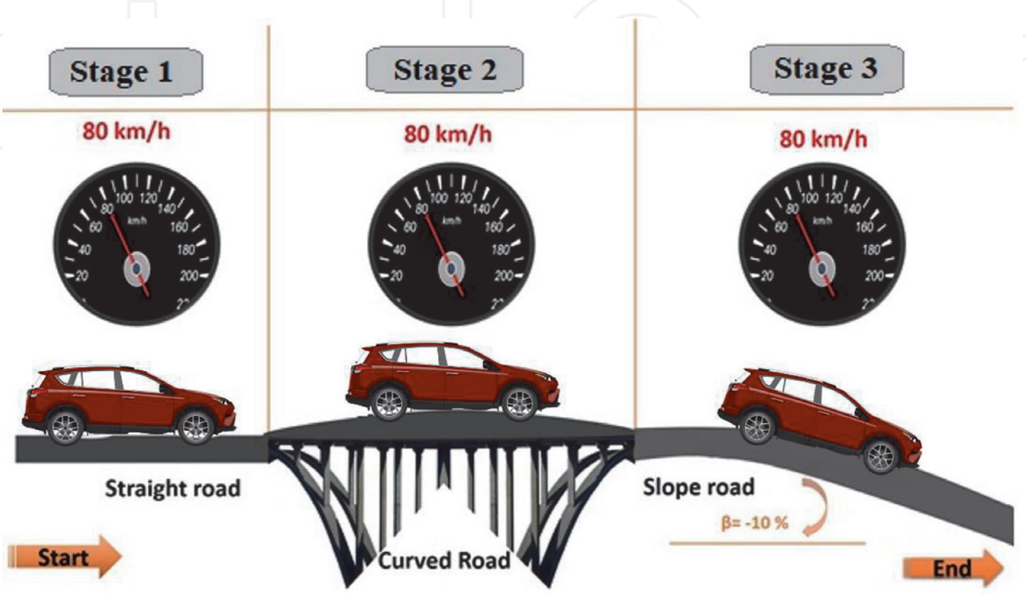

Figure 38.
Driving cycle of the EV includes three stages.

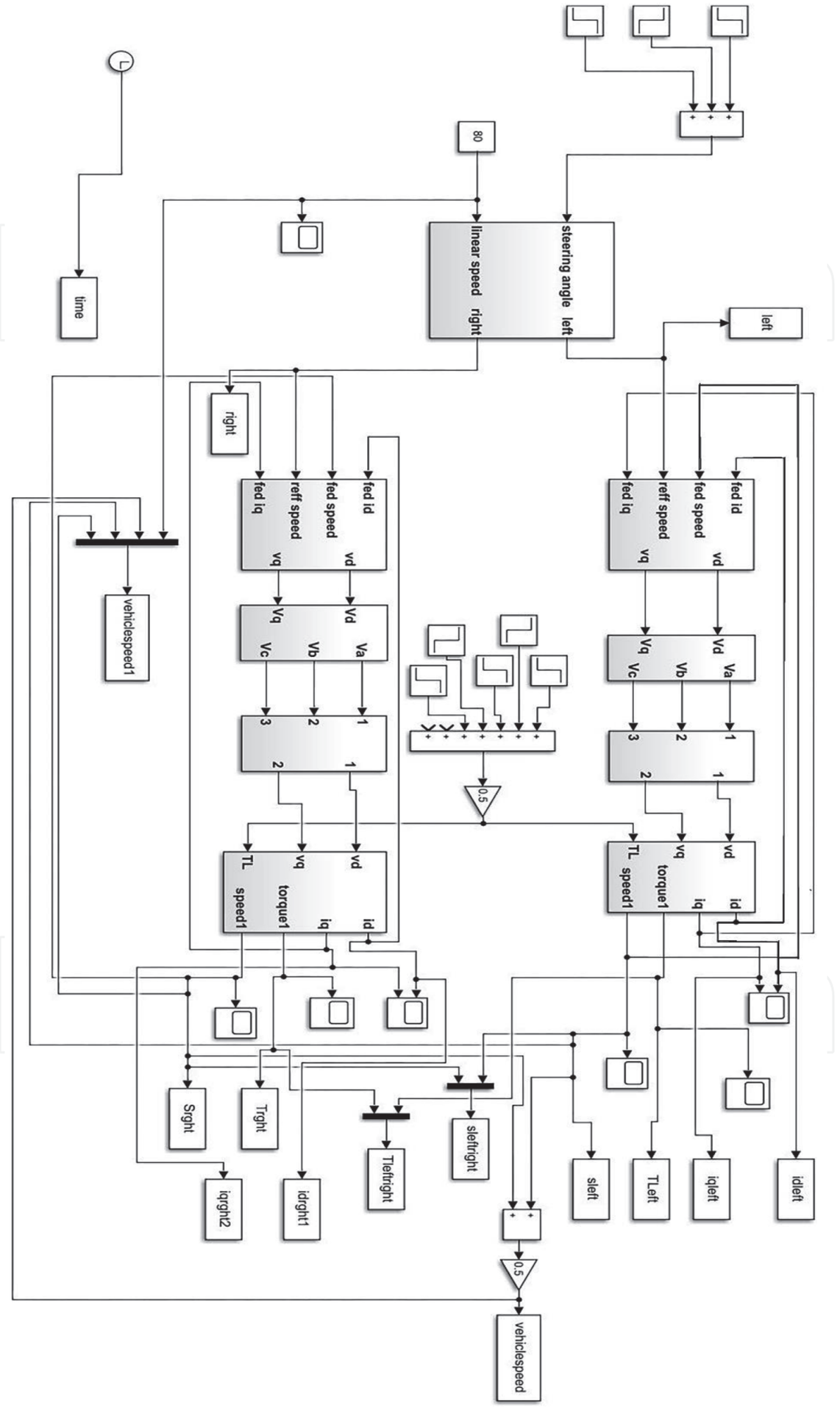

Figure 39.
Modeling and simulation of PEV model.

DOI: http://dx.doi.org/10.5772/intechopen.98873

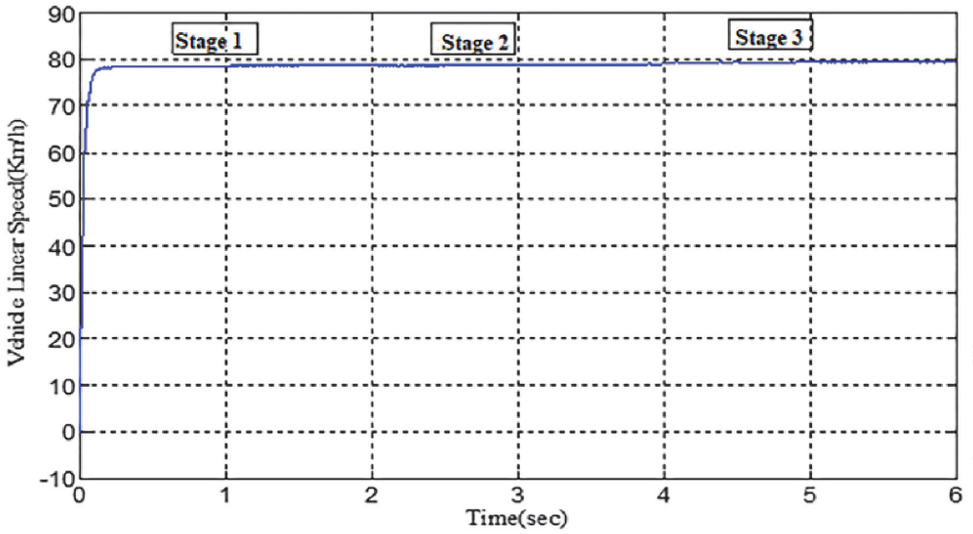

Figure 40.
The linear speed of the EV.

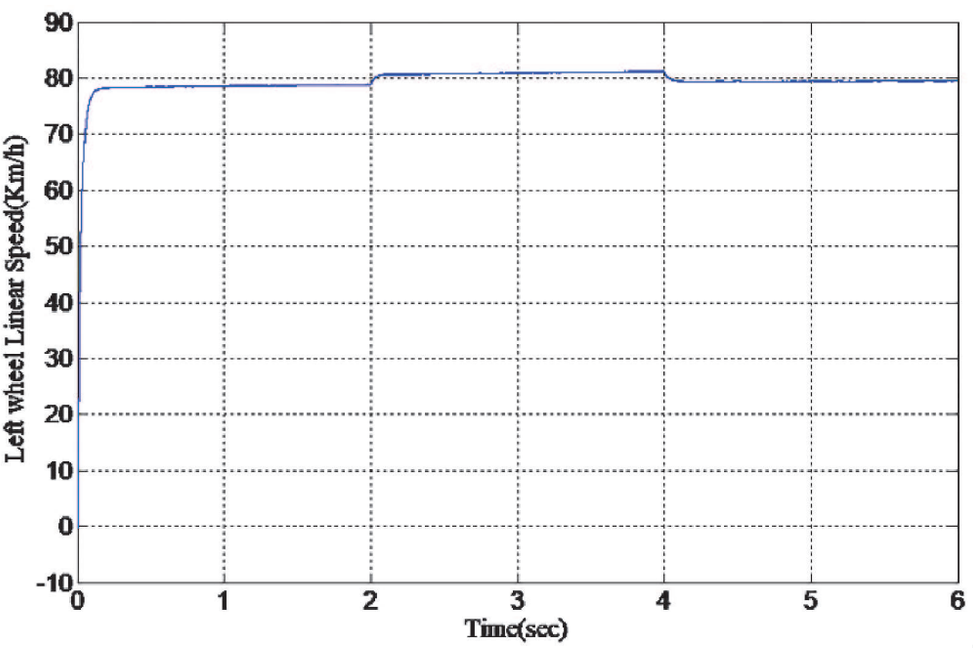

Figure 41.
The linear-speed at the left-wheel of the EV.

- The 1st stage: the EV moving in the straight road along with the moving beginning with the next zero and finish in the next two of the estimated time.

- The 2nd stage: that the EV turns directly from the curve street with 2.5 levels of the steering wheel along with the moving beginning from two minutes two and finish with the next four of the projected periods.

- The 3rd stage: that the EV descents in off-road street with 10 degrees of incline angle and the moving start from the next four and end with the next six of the estimated periods.

Figure 39 shows the full design of the EV consists of all main parts in this chapter. Besides, it explained the connecting ways between them to get the full system simulation.

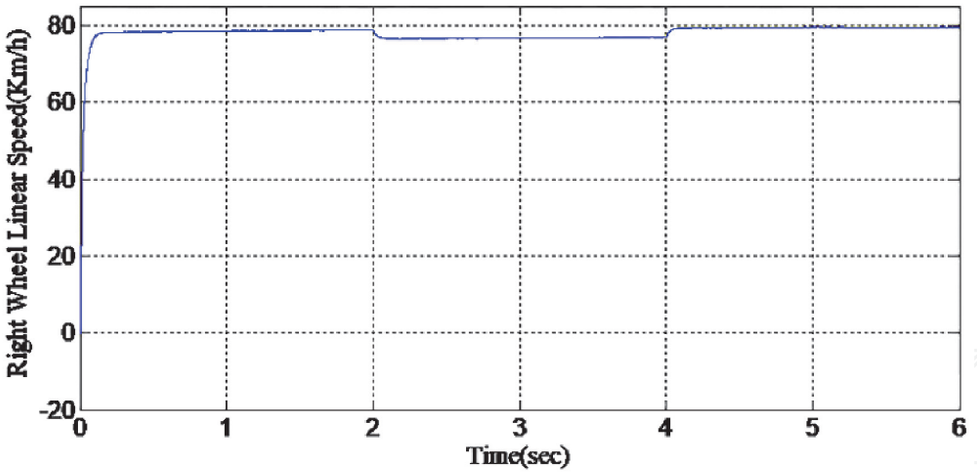

Figure 42.
The linear-speed at the left-wheel of the EV.

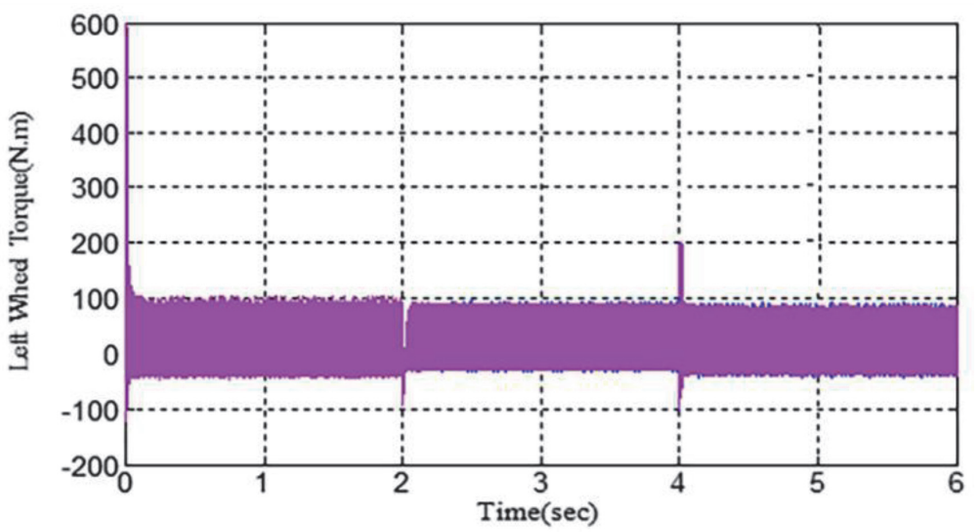

Figure 43.
The torque at the left-wheel of the EV.

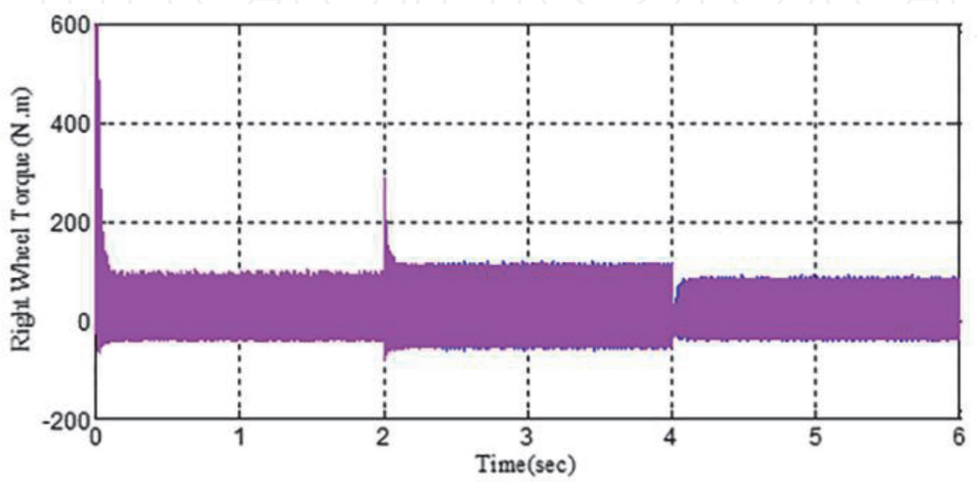

Figure 44.
The torque at the right-wheel of the EV.

The time	From 0 to 4 second	From 4 to 6 second
The load	32.52 Nm	25 Nm

Table 8.
The load information's for the driving cycle.

The result of the simulation the first drive cycle that have referred to the **Figure 40** for each stage is explained in the points below:

Figure 41 represent the linear speed of the EV that is started from zero to reach the 77 km/h in stage1 in the next one and continued to reach at the 78.5 km/h at 2nd stage in the second two of the moving time also continue to reach the 80 km/h in the next four of the transferring time in the previous step of simulation in the slop road.

Figure 42 reflect the linear speed of the wheel of the EV that has started from zero to reach the 77 km/h in 1st stage in the next one and grow up to achieve the 83 km/h in the stage 2 since the EV has turned into and this point indicates the influence on the left wheel of this EV. The last point after the decease to reach the 80 km/h in simulation in the slop street.

Figure 43 reflect the linear speed of the right wheel of this EV that's started from zero to reach the 77 km/h in stage1 from the 2nd second and decease to 75 km/h at the 2nd stage since the EV has flipped directly which stage indicates the influence of the ideal wheel of the EV. In the 3rd stage after the decease to reach the 80 km/h at of simulation in the slop road.

Figure 44 represents the torque of the left wheel of the EV. The torque has already now reached 600 N.m at the first moment of the EV moving in stage1 then decease to be stable in 200 N.m throughout this stage. In the second two of those moving represent the 2nd stage of the simulation, the torque decease to 50 N.m due to the curve road then grew to become stable in 200 N.m in this stage. The second four reflect that the 3rd stage and the torque increase up to 600 N.m only at that second and then reduction to be stable in 188 N.m in the slop road.

The torque has already reached 600N.m at the very first moment of the EV moving-in stage1 after that decease to be stable in 145 N.m in this stage. At the next two of the moving represent that the 2nd stage of the simulator, the torque growth to 300 N.m due to this curve road after that increase to become stable at 180 N.m with this stage. The 3rd stage starts from the second four of their transferring periods and the torque decease to 50 N.m because of the curve road after that rise to attain and become stable at 150 N.m. The loaded that effect on the EV for each stage is represented in **Table 8**.

7. Conclusion

The EDC symbolizes the gearbox as positioned in electric vehicles which operate the transferring, the rate and transform the direction by the wheels into the fundamental engines accountable for providing the wheels of their EV using adequate torque for spinning along with forcing the EV. Besides this gadget controls the angle of the EV making it stable at the guide roads and alternative methods which have been mimicked by hypotheses in the research. Thus, the EDC-technology has really used to restrain the linear rate of their EV and confirm the vehicle equilibrium under several street states as exhibited in section.

The EDC topology has implemented in this simulation to test the stability and functionality of their EV under several street situations and road angles. Additionally, the simulator comprises three various drive-cycles each drive cycle includes many

stages with various road-condition. The linear rate of the EV might be computed by locating the result of the left and right wheel's linear rates. The driving cycle shows the EV balance across the whole cycle to make it to the close of the cycle.

According to the simulation result, the EV structure has stability and higher response in several distinct states with 80 km/h highest speed at the right road. Additionally, to guarantee the security of the function of the electric apparatus in the genuine electric vehicle must be analyzed separately on the simulators restrain the wheel of the EV along with also the angle of deviation of the vehicle by implementing different torque rates as shown in the simulator amounts.

Acronyms and abbreviations

T	The electromagnetic torque of SynRM in $\mathbf{N/m}$
$\mathbf{P}$	The number of poles of SynRM
$\mathbf{J}$	The moment of inertia coefficient of the motor in $(\mathbf{K_g M^2})$
$\mathbf{T_L}$	The inside load torque of SynRM $(\mathbf{N/m})$
$\mathbf{B}$	The viscous friction coefficient of SynRM
N	The number of the space vector sectors
$\mathbf{k_p}$	Proportional gain
$\mathbf{k_i}$	The integral gain
$\mathbf{k_d}$	The derivative gain
$e(t)$	The error
$\mathbf{M_p}$	The overshoot
$\mathbf{y(i)}$	The model output
$\mathbf{D(i)}$	The wanted output
$\mathbf{n}$	The actual speed
$\mathbf{n_{ref}}$	The reference speeds
$\mathbf{v_i(t)}$	The velocity
$\mathbf{x_i(t)}$	The current position
x_i^k	The current position of particle (i) at iteration (k)
v_i^k	The velocity of particle(i) at iteration (k)
w	The inertia weight
c_1, c_2	The positive acceleration constants
R_1, R_2	are random variables distributed uniformly in the range [0; 1]
w_{min}	The inital weight
w_{max}	The final weight
$iter_{max}$	The maximum iteration numbers.
V_L ann V_R	The linear speed of the the left and right wheels of the EV in (km/h)
ω_v	The liner speed of the EV in (Km/h)
d_ω	The size width of EV in (meter). R the road curve
L_ω	The EV length and δ is the street angle
m	The total mass of the EV in(kg)
g	The gravity acceleration in (m/s)
f_r	The rolling resistance force constant.
ρ_{air}	The density of air in (k_g/m^3)
A_f	The frontal surface area in (m^2)
C_d	The aerodynamic drag coefficient
V	The linear speed of the vehicle in (km/h)
β	The slope angle of the street
ω_z	The zero of Led-leg compensator
ω_p	The pols of Led-leg compensator

DOI: http://dx.doi.org/10.5772/intechopen.98873

Author details

Muhammet Tahir Guneser*, Mohammed Ayad Alkhafaji and Cihat Seker
Karabuk University, Karabuk, Turkiye

*Address all correspondence to: mtguneser@karabuk.edu.tr

References

[1] İnci, Büyük M, Demir M H, İlbey G. Mint: A review and research on fuel cell electric vehicles: Topologies, power electronic converters, energy management methods, technical challenges, marketing and future aspects. ELSEVIER. 2021;36: 130-141. Doi: org/10.1016/j.egypro.2013.07.016

[2] Xu Y, Zheng Y, Yang Y. Mint: On the movement simulations of electric vehicles: A behavioral model-based approach. ELSEVIER. 2021; 283: 0306-2619. Doi: org/10.1016/j.apenergy.2020.116356.

[3] Agamloh E, von Jouanne A, Yokochi A. Mint: An Overview of Electric Machine Trends in Modern Electric Vehicles machines. MDPI AG. 2020; 8(2): 20. doi.org/10.3390/machines8020020

[4] AlKhafaji M A, Uzun, Y. Simulation and control of an electric vehicle by using PSO and specify driving route topology. In: Proceedings of the IEEE International Conference on Power Generation Systems and Renewable Energy Technologies (PGSRET); 1-6, August 2019; Istanbul. Turkey.

[5] Güneşer, M T, Dalcalı A, Özturk T, Ocak C. Influence of Rotor Slot Structure at Starting Torque and Efficiency on Urban Use EV Motor. IN: Proceedings of the IEEE International Conference on Power Generation Systems and Renewable Energy Technologies (PGSRET); 1-4, August 2019. Istanbul. Turkey IEEE.

[6] AlKhafaji M A, Uzun, Y. Design and Speed Control of SynRM Using Cascade PID Controller with PSO Algorithm. In: International Journal of Renewable Energy Development (IJRED); 69-76, February, 2020. Ispanya. Madrid.

[7] AlKhafaji M A, Uzun, Y. Design, simulation and analysis of synchronous reluctance motor, The International conference on innovative research in Science Engineering and Technology (IRSET). 2018, Belgrade, Serbia.

[8] Thounthong P, Sikkabut S, Poonnoy N, Mungporn P, Yodwong B. Kumam P, Bizon, Nahid-Mobarakeh B, Pierfederici S. Mint: Nonlinear differential flatness-based speed/torque control with state-observers of permanent magnet synchronous motor drives. IEEE Transactions. 2018; 2874-2884. DOI: 10.1109/TIA.2018.2800678.

[9] Tildirim M. and Kurum,H. Electronic Differential System for an Electric Vehicle with Four In-wheel PMSM. IN: Proceedings of the IEEE 91st Vehicular Technology Conference (VTC2020-Spring); 1-5. May 2020; Antwerp. Belgium.

[10] Yıldırım M. Öksüztepe E. Tanyeri B. Kürüm H. Electronic differential system for an electric vehicle with in-wheel motor. IN: Proceedings of the IEEE International Conference on Electrical and Electronics Engineering (ELECO); 1048-1052. November 2015; Bursa. Turkey.

[11] Zhang N, Xu C, Niu W, Lu X. The electronic differential control based on the slip ratio. IN: Proceedings of the IEEE 36th Chinese Control Conference (CCC); 9384-9389. July 2017. Dalian. China.

[12] Abdul-hassan, K M, Kahdum S A. Simulation of Speed Control for Synchronous Reluctance Motor Based on Tuning Cascaded PID Controller with PSO Algorithm. IN: Proceedings of University of Thi-Qar Journal for Engineering Sciences; 1-15. November 2016. Thi-Qar. Iraq.

[13] Gasbaoui B, & Nasri A. The uses of artificial intelligence for electric vehicle

control applications. In: Subhas Chakravarty, editors. Technology and Engineering Applications of Simulink. 2012. P. 239-256. DOI: 10.5772/36653. ch11

[14] AlKhafaji M A, Uzun, Y. Modeling and Simulation of A Photovoltaic Cell Module Controlled with Nonlinear Autoregressive Moving Average-L2 Controller. IN: Proceedings of the IEEE International Conference on Electrical, Communication, and Computer Engineering (ICECCE); 1-5. June 2020; Istanbul. Turkey.

[15] Hartani K, Bourahla M, Miloud Y, Sekour M. Mint: Electronic differential with direct torque fuzzy control for vehicle propulsion system. Turkish Journal of Electrical Engineering & Computer Sciences. 2009; 21-38. DOI: 10.3906/elk-0801-1

[16] Fellani, M A, Abaid E. Mint: Modeling and Simulation of Reluctance motor using digital computer. IJCSEE; 2013; 2:148-52. ISSN 2320–4028

[17] Roukas, M. Development of the control system for an electric vehicle [Thesis]. Göteborg, Sweden: Chalmers University of Technology; 2013

[18] Mebarki, B, Draoui B, Rahmani L, & Allaoua B. Mint: Electric automobile Ni-MH battery investigation in diverse situations. Energy Procedia, 2013; 36: 130-141. DOI: org/10.1016/j. egypro.2013.07.016

[19] Pesce, T, Lienkamp M. Mint: Definition and optimization of the drive train topology for electric vehicles. World Electric Vehicle Journal. 2012; 5: 24-35. Doi: org/10.3390/wevj5010024

[20] Daya J F, Sanjeevikumar P, Blaabjerg F, Wheeler P W, Ojo J O. Mint: Implementation of wavelet-based robust differential control for electric vehicle application. IEEE Transactions. 2015; 30: 6510-6513. DOI:10.1109/ TPEL.2015.2440297.

[21] Jazar R N. Handbook of Forward Vehicle Dynamics. 2nd ed. Springer: Cham; 39-97 p. DOI: 10.1007/978-3-319-53441-1_2

[22] Roukas M. Development of the control system for an electric vehicle [thesis]. Göteborg, Sweden: Chalmers University of Technology; 2013.

[23] Sathyan S. Synchronous reluctance motor for household applications [thesis]. Espoo, Finland: AALTO University School of Electrical Engineering; 2013.

[24] Boyd S J, Nelson D. Hybrid electric vehicle control strategy based on power loss calculations hybrid electric vehicle control strategy based on power loss calculations [thesis]. Blacksburg, USA: Virginia Polytechnic Institute and State University; 2006.

[25] Kazmierkowski M P. Handbook of Automotive Power Electronics and Motor Drives. 2nd ed. Emadi, A: IEEE Industrial Electronics Magazine; 2006. 46-47 p. DOI: 10.1109/MIE.2008. 926483.

[26] Rahimian M S, Raahemifar K. Mint: Optimal PID controller design for AVR system using particle swarm optimization algorithm. IEEE Ccece. 2011; 337-340. DOI: 10.1109/ CCECE.2011.6030468.

[27] Ravi A, Palani S. Mint: Robust electronic differential controller for an electric vehicle. American Journal of Applied Sciences. 2013;10(11), 1356.

[28] Tran P H. Matlab/Simulink implementation and analysis of three pulse-width-modulation, [thesis]. Boise, Idaho: Boise State University; 2012.

[29] Salem, F A. Mint: Modeling and control solutions for electric vehicles.

ESJ. 2013; 9,15: 1857-7881. DOI: 10.19044/esj. 2013.v9n15p%25p

[30] Du J, Ouyang M, Chen J. Mint: Prospects for Chinese electric vehicle technologies in 2016–2020: Ambition and rationality. ELSEIER Energy. 2017; 120: 584-596. DOI: 10.1016/j. energy.2016.11.114.

[31] GÜNEŞER M T, Erdil E, Cernat M, ÖZTÜRK T. Mint: Improving the energy management of a solar electric vehicle. AECE. 2015; 4: 53-62. DOI:10.4316/ AECE.2015.04007.